

CO<sub>2</sub> TO NATURAL GAS (CH<sub>4</sub>) CONVERSION IN METHANOGEN-MINERAL  
SYSTEMS: THE ROLE OF MINERAL TYPE

by

PATRICK BOND LAZZARINO

Bachelor of Science, 2015  
University of Southern Mississippi  
Hattiesburg, Mississippi

Submitted to the Graduate Faculty of the  
College of Science and Engineering  
Texas Christian University  
in partial fulfillment of the requirements  
for the degree of

Master of Science

December 2017

CO<sub>2</sub> TO NATURAL GAS (CH<sub>4</sub>) CONVERSION IN METHANOGEN-MINERAL  
SYSTEMS: THE ROLE OF MINERAL TYPE

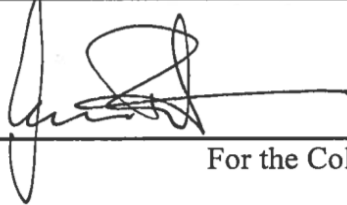
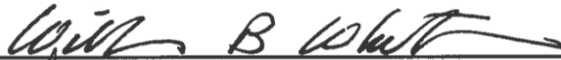
by:

Patrick Lazzarino

Thesis approved:



Major Professor



For the College of Science and Engineering



## ACKNOWLEDGEMENTS

I would like to acknowledge my advisor Dr. Omar Harvey for giving me the opportunity to work with him on some novel research while earning my Masters. Also, this work would not have been possible without the help of Dr. William “Barny” Whitman and his lab assistants (Especially Zhe Lyu, Taiwo Akinyemi, and Feng Long) at the University of Georgia. They not only taught me how to grow our archaea, but helped me gain a general comfort inside of a biology laboratory. Thank you to Dr. Kayla Green and her Graduate Assistant Samantha Brewer for help with the anaerobic chamber. I would also like to thank Dr. Ken Jarrell at Queen’s University for being generous enough to send us our sample strains of *M. maripaludis*. Dr. Clark Jones for help with the autoclave and incubator room. Also, Milt Enderlin must be thanked for always helping me with equipment needs and bouncing ideas in general. Thank you to Burke Leonce for keeping me sane my first year. Finally, I would like to thank my parents and my brother for always supporting me and allowing me the flexibility to pursue my research.

## TABLE OF CONTENTS

ACKNOWLEDGEMENTS .....	ii
LIST OF FIGURES .....	v
LIST OF TABLES .....	vi
1. RESEARCH MOTIVATION AND PREMISE .....	1
2. LITERATURE REVIEW .....	3
3. MATERIAL AND METHODS .....	9
3.1 Mineral Selection and Preparation .....	9
3.2 Sample Strain Cultivation .....	10
3.3 Assessment of mineral effects on CO <sub>2</sub> -to-CH <sub>4</sub> conversion by <i>M. Maripaludis</i> .....	11
3.4 Headspace Gas Sampling and Analysis .....	14
4. RESULTS .....	16
4.1 Mineral electrical conductivity (EC <sub>min</sub> ) effects on CO <sub>2</sub> -to-CH <sub>4</sub> conversion ratio (R <sub>CH4</sub> ) by <i>M. maripaludis</i> .....	16
4.1.1 Insights on EC <sub>min</sub> -R <sub>CH4</sub> relationship from experiments in H <sub>2</sub> -rich environments .....	16
4.1.2 Insights on EC <sub>min</sub> -R <sub>CH4</sub> relationship from experiments in H <sub>2</sub> -limited environments .....	21
4.1.3 Summary of general trend analysis for Experiment 1 .....	25
4.2. Minerals effects on kinetics of CO <sub>2</sub> -to-CH <sub>4</sub> conversion .....	26
4.2.1 Temporal trends and kinetics of CO <sub>2</sub> -to-CH <sub>4</sub> conversion.....	27
5. CONCLUDING REMARKS.....	32
Appendix A: Detailed growth media preparation for <i>M. maripaludis</i> .....	34
Appendix B: pH values for varying mineral treatments for Experiment 1.....	38

Appendix C: Overall CH <sub>4</sub> and CO <sub>2</sub> Concentrations on Day 14 (%).....	40
References .....	42
Vita	
Abstract	

## LIST OF FIGURES

Figure 1. Electrical conductivity of rock units in $\text{mS m}^{-1}$ .....	9
Figure 2. Experimental Setup in Anaerobic Chamber .....	13
Figure 3. Sealed and crimped reactors .....	13
Figure 4. Incubation of reactors .....	14
Figure 5. Gas chromatograph injection for calibration gas and samples .....	15
Figure 6. $R_{CH_4}$ for wild-type <i>Mm900</i> with varying mineral type in $\text{H}_2/\text{CO}_2$ .....	16
Figure 7. $R_{CH_4}$ for non-archaeallated $\Delta\text{flaB2}$ with varying mineral type in $\text{H}_2/\text{CO}_2$ .....	18
Figure 8. Day 1 $R_{CH_4}$ as a function of mineral electrical conductivity in $\text{H}_2$ -rich conditions .....	19
Figure 9. $R_{CH_4}$ for wild-type <i>Mm900</i> with varying mineral type in $\text{N}_2/\text{CO}_2$ .....	21
Figure 10. $R_{CH_4}$ for non-archaeallated $\Delta\text{flaB2}$ with varying mineral type in $\text{N}_2/\text{CO}_2$ .....	23
Figure 11. Day 1 $R_{CH_4}$ as a function of electrical conductivity in $\text{H}_2$ -limited conditions .....	24
Figure 12. Kinetics of $\text{CO}_2$ -to- $\text{CH}_4$ conversion ( $R_{CH_4}$ ) in $\text{H}_2$ -rich and $\text{H}_2$ -limited environments with wild-type <i>Mm900</i> and non-archaeallated $\Delta\text{flaB2}$ .....	28

## LIST OF TABLES

Table 1. Equations for $R_{CH_4}$ -log ( $EC_{min}$ ) relationships for <i>Mm900</i> and $\Delta flaB2$ in H <sub>2</sub> -rich and H <sub>2</sub> -limited environments on days 1 and 14 .....	21
Table 2. Day 14 equations and fits for $R_{CH_4}$ -log ( $EC_{min}$ ) relationships for <i>Mm900</i> and $\Delta flaB2$ in H <sub>2</sub> -rich and H <sub>2</sub> -limited environments .....	25
Table 3. Modeled parameters max conversion (c), rate constant (k), and half-life ( $t_{1/2}$ ) with r <sup>2</sup> values .....	29



## 1. RESEARCH MOTIVATION AND PREMISE

Since the mid-19<sup>th</sup> century, atmospheric carbon dioxide (CO<sub>2</sub>) levels have increased from less than 300 ppm to more than 400 ppm.<sup>1</sup> With more than 3.2 gigatons of CO<sub>2</sub> released annually, contributions from anthropogenic fossil fuel burning continues to be the primary source of excessive CO<sub>2</sub> inputs into the atmosphere.<sup>2</sup> As methods for discovery and recovery of oil and gas continue to be improved, fossil fuels are likely to remain a cheap energy source relative to current renewable energy strategies. The use of fossil fuels will therefore continue to be a big part of our energy strategy into the foreseeable future and consequently will continue to negatively impact atmospheric CO<sub>2</sub> levels. Given current infeasibility in reducing atmospheric CO<sub>2</sub> levels via substantial reductions in fossil fuel use, mitigation strategies will need to include capacity to store large amounts of carbon dioxide from major CO<sub>2</sub> emitters.

In recent years, the capture and storage of CO<sub>2</sub> from the largest point source emitters in deep geological formations has emerged as the most promising mitigation strategy. This strategy, often referred to as geological CO<sub>2</sub> sequestration (GCS) or Carbon Capture Storage (CCS), has several advantages: 1) the technology needed is available and mature (the energy industry has been storing (and extracting) gases in (from) geological formations for decades, 2) the storage capacity needed is available (storage capacity in known suitable geologic formations within the conterminous US can hold all the CO<sub>2</sub> projected to be produced from fossil fuels over the next 2 centuries<sup>3</sup>, 3) environmental impacts are fairly well understood, can be assessed and minimized<sup>4,5</sup> and 4) there are significant value-added potential both economically and scientifically.

The reality is that GCS is expensive and current government incentives in most instances are inadequate to encourage large-scale adaptation. This has led to calls from key

stakeholders (including the US Department of Energy) for the focus of CCS to be shifted from mere CO<sub>2</sub> capture and storage towards CO<sub>2</sub> utilization as an input/feedstock for value-added processes. This addition of the “utilization” component to CCS (now CCUS) has seen successful efforts being made in the use of CO<sub>2</sub> in energy production efforts such as; enhanced oil recovery (CO<sub>2</sub>-EOR) and enhanced coal-bed methane recovery (ECBM). Unmineable coal seams and oil/gas fields that were once considered non-economical have seen increases in productivity of 30-50 and 30-65 percent, respectively.<sup>6-8</sup> Although very positive for the overall value-added outlook of CCUS, CO<sub>2</sub>-EOR and ECBM are limited by the fact that most of the available storage capacity for CO<sub>2</sub> is located in geological formations that contain no oil or coal-bed methane. Instead, the vast majority of CO<sub>2</sub> storage capacity is located in deep-saline aquifers with waters that are deemed too saline for domestic use and/or too uneconomical to pump.<sup>9, 10</sup> One possibility for adding value to CCUS in these deep saline aquifers is the enhanced conversion of CO<sub>2</sub> to methane (CH<sub>4</sub>; the main component in natural gas) via autotrophic methanogenesis; with the subsequent utilization of the natural gas produced for energy generation.

The ubiquity of deep-saline aquifers and the widespread occurrence of microbial-mediated autotrophic methanogenesis in deep geologic environments<sup>11, 12</sup> mean that the probability for locating enhanced CO<sub>2</sub>-to-natural gas projects close to major point-source, CO<sub>2</sub> emitters (e.g. fossil-fuel-fired power plants and factories) are great. So too is the potential for incorporating the produced natural gas into a closed-loop hybrid power generation system; with CO<sub>2</sub> from the point source being pumped into the aquifer at one end and the natural gas produced (from enhanced CO<sub>2</sub>-to-natural gas conversion) being used in part or full to power the plant or factory. Another associated benefit of enhanced CO<sub>2</sub>-to-

natural gas conversion is the enhanced mineral trapping of CO<sub>2</sub>, as a structural component, in carbonate minerals. Harvey *et al.*<sup>13</sup> recently showed that the formation of iron-carbonate was enhanced in the presence of autotrophic methanogenesis but was absent from treatments without methanogenesis. The formation of carbonates from CO<sub>2</sub> is important because it results in the permanent sequestration of CO<sub>2</sub> in stable mineral deposits.

Despite the framework of methanogenesis-facilitated CCUS being plausible, the fundamental science needed to make this work is still in its infancy. For example, subsurface storage sites exhibit a great deal of heterogeneity with respect to mineral composition, pressure, temperature, and biological activity.<sup>2</sup> However, there is very little current research that integrates these factors. This research effort is intended to contribute to the fundamental science components needed to support a framework for enhanced CO<sub>2</sub>-to-natural gas conversion as a value-added component in CCUS. Specific objectives will be: 1) to assess the effect of mineral electrical conductivity on the kinetics of CO<sub>2</sub>-natural gas conversion; 2) to determine differences in rock/mineral interactions based on morphological characteristics (*flagellated/ non-flagellated*) in order to better understand possible electron transfer mechanisms.

## **2. LITERATURE REVIEW**

One limiting factor of synthetic conversion of CO<sub>2</sub> to CH<sub>4</sub> (autotrophic methanogenesis) is overcoming the very negative redox potential (-240 mV) of the reaction which requires catalysts and high energy input to produce substantial amounts of CH<sub>4</sub>.<sup>14</sup> Methanogenic archaea and bacteria are capable of overcoming this low potential by utilizing enzymes to facilitate CO<sub>2</sub> to CH<sub>4</sub> conversion in naturally-occurring reduced environments (subsurface geologic sites, anaerobic marshes, etc.) In addition to naturally-occurring

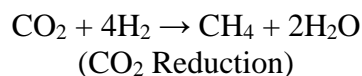
enzymes, several metals and metal oxides have been shown to increase rates of conversion by possibly acting as reducing-agents for these reactions in laboratory experiments.<sup>15, 16</sup>

Several studies in the 1980's and 90's focused on the impacts of metal pollution on methanogenesis in marine environments. Capone *et al.*<sup>14</sup> studied the effects of a large suite of alkaline earth and transition metals on methanogenesis in homogenized salt marsh sediments. Most metals tested were found to enhance methanogenesis (after an initial lag time) with molybdenum ( $\text{Na}_2\text{MoO}_4$ ) showing the greatest increase in maximum  $\text{CH}_4$  production (23-fold increase in  $\text{CH}_4$ ) compared to controls containing no metals. The increase in methanogenesis observed in these experiments was attributed to metal-related inhibition of  $\text{SO}_4^{2-}$ -respiring bacteria found in these syntrophic systems.<sup>15</sup> Lorowitz *et al.*<sup>15</sup> expanded on this research and tested the response of a single autotrophic species (*Methanobacterium thermoautotrophicum*) to a wide suite of elemental metals. This study showed that many metals could act as electron donors for this species significantly enhancing  $\text{CH}_4$  production; for example, magnesium treatments had 954  $\mu\text{mol}$ , iron treatments had 415  $\mu\text{mol}$ , and zinc treatments 85  $\mu\text{mol}$  compared with 0.76  $\mu\text{mol}$  for control reactors. This study was important in showing that at least one species of autotrophic methanogen can utilize free electrons created by metals via a process known as cathodic depolarization.<sup>16</sup> It has been proposed that elemental metals can be oxidized in these aqueous environments which releases hydrogen that can be used in methanogenesis.

*Methanococcus maripaludis* is a hydrogenotrophic archaea which thrives in strictly anaerobic environments such as deoxygenated swamps, subsurface pore space, and hydrocarbon reservoirs.<sup>17</sup> In these oxygen-poor environments, *M. maripaludis* has the ability to utilize seven different hydrogenases to convert  $\text{H}_2$  gas into free electrons, which are then

used to reduce CO<sub>2</sub> to CH<sub>4</sub>.<sup>18</sup> The ability of this species to utilize simple carbon (CO<sub>2</sub> and formate) and nitrogen (N<sub>2</sub>) substrates has spurred widespread interest for its potential use in carbon sequestration efforts. In addition, the optimal growth temperature is lower than many methanogenic species (37°C) and its growth rate (Population doubling time = 2 hrs.) is one of the fastest amongst methanogens making it a widely used model species.

*M. maripaludis* is small (0.9-1.3 µm) with a coccus structure which has two types of surface appendages: archaeal flagella (archaella) and pili.<sup>19</sup> The archaella have been shown to aid in motility in addition to surface attachment. Although pili appendages have not been as extensively studied in *M. maripaludis*, recent evidence suggests that both appendages are necessary for strong attachment to inorganic surfaces.<sup>20</sup> Methanogenesis is the primary metabolism for the species as well as the only means of energy production for growth leading to competition for carbon resources.<sup>18</sup> It occurs via two mechanisms: disproportionation of formate or reduction of CO<sub>2</sub> with an electron donor such as hydrogen, formate, or electricity which can be shown in the simplified equations below:<sup>18, 21</sup>



Although it has been studied for decades, the primary focus has been on genetic sequencing and alteration as well as its interactions with syntrophic organisms which aid in methanogenesis by means of extracellular electron transfer (EET)<sup>22</sup>. The studies that have incorporated metals and minerals with methanogens were primarily focused on environmental impacts regarding stimulatory effects on GHG's. However, recent research has shifted focus to the usefulness of methanogenic archaea such as *M. maripaludis* as

biological tools in mitigation efforts against climate change and specifically for CCUS. As mentioned earlier, methanogens have been shown to facilitate in the precipitation of iron-carbonate which could be useful in converting and storing large amounts of CO<sub>2</sub> without significant surface impact on the environment.<sup>13</sup> Additionally, as populations grow wastewater treatment will continue to utilize methanogens for energy generation, which will be crucial to maintaining healthy urban societies in the future.<sup>23, 24</sup> Finally, if natural gas prices were to increase or if the release of CO<sub>2</sub> were to become prohibitively expensive, methanogenic recovery of CH<sub>4</sub> from carbon sequestration may prove profitable in the future.<sup>25</sup>

Recent evidence has shown that differences in mineral conductivity affects kinetic rates of conversion in soil settings. Kato *et al.*<sup>26</sup> and Zhou *et al.*<sup>27</sup> showed that methanogenesis in soils can be significantly influenced by the presence of semi-conductive iron oxide minerals. In these experiments, iron oxide minerals [ferrihydrite (5Fe<sub>2</sub>O<sub>3</sub>·9H<sub>2</sub>O), hematite (Fe<sub>2</sub>O<sub>3</sub>), and magnetite (Fe<sub>3</sub>O<sub>4</sub>)] were added to rice paddy soils in the presence of a methanogens from the genus *Methanosarcina* as well as syntrophic *Geobacter* species. Both experiments saw higher rates of methanogenesis in treatments containing minerals with higher Electrical Conductivity (EC). Zhou *et al.* showed increases in CH<sub>4</sub> production from 82.8 μmol in non-mineral controls to 172.9 μmol and 299.0 μmol in the presence of hematite (EC = 3.45 x 10<sup>-3</sup> mS m<sup>-1</sup>) and magnetite (EC = 4.09 x 10<sup>-3</sup> mS m<sup>-1</sup>), respectively. In contrast, there was significantly less CH<sub>4</sub> produced in the presence ferrihydrite (EC = 2.69 x 10<sup>-3</sup> mS m<sup>-1</sup>) at 19.1 μmol CH<sub>4</sub>. In addition to soil settings, metal amendments have also been shown to increase methanogenesis in anaerobic wastewater digesters which use methanogenic archaea to create CH<sub>4</sub> from organic waste extracted from wastewater. Feng *et*

*al.* (2014) showed increases in CH<sub>4</sub> production of 43.5% when digesters were amended with zero-valent iron. Elemental manganese [Mn(0)] has also been shown to increase both rates and overall production of CH<sub>4</sub> in wastewater digesters. In 2015, Qiao *et al.* showed a rate increase in syntrophic acetivlastic methanogenesis of 3.5-fold and an overall production increase of 2.7-fold with respect to controls for amended treatments. One important finding from this study is that increases in production/activity were not directly linked to increases in concentrations of metals. (4 g/L > 8 g/L > 2 g/L). As mentioned before, it has been proposed that methanogens can use these metals/minerals as conduits for shuttling electrons during extra-cellular interspecies interactions during syntrophic methanogenesis.<sup>26, 28, 29</sup> In addition, autotrophic methanogenesis enhancement with elemental metals via cathodic depolarization has been proposed for decades based on the indirect evidence for this mechanism.<sup>30</sup>

There are no current studies, or at least to our knowledge, on intra-species shuttling of electrons or cathodic depolarization in methanogenesis in *M. maripaludis*. A large part of this may be attributed to the fact that, up until very recently, much of the research on methanogens (and particularly *M. maripaludis*) has focused on genetic sequencing and interspecies interactions. It can be reasonably inferred that if minerals have such drastic effects on methanogenic processes in marshes, soils, and wastewater, they must have some effect on subsurface methanogenesis where microbial communities have much greater contact with mineral surfaces. Since subsurface storage sites vary greatly in mineral composition (i.e. mineral conductivity), it is important to begin understanding the relationships between microbial communities and their surrounding environments. Although recent studies have introduced the relationships between minerals and syntrophic

methanogenic systems, few have focused on mineral/methanogen interactions in the absence of syntrophic organisms. Doing this, will determine whether methanogens themselves can use electrically conductive mineral surfaces to grow and/or increase methane production.

Although CO<sub>2</sub> methanogenesis occurs mostly via indirect hydrogenase-dependent mechanisms, recent evidence suggests that an alternative hydrogenase-independent pathway exists which may directly uptake electrons. A 2014 study by Lohner *et al.* reported methanogenesis in reactors containing *M. maripaludis* with genes omitted for hydrogenase production. In this study, hydrogenase-deleted mutants were able to draw electrons directly from an electrode at a rate of 1/10 of the rates observed in wild-type reactors<sup>21</sup>. While this pathway is not well understood, it is possible that microbial communities are using this mechanism to shuttle electrons across conductive mineral surfaces in the absence of electron donors such as hydrogen gas. Jarrell *et al.* reported that both pili and archaeella are needed for attachment to mineral surfaces, but the range of uses for these appendages remains uncertain.<sup>20</sup> By deleting genes necessary for forming these appendages, they were able to show that wild-type *Mm900* was able to attach to different inorganic surfaces (gold, nickel, molybdenum, glass) whereas mutants without pili and/or archaeella did not attach readily to any surface. Since it is known that these appendages are used for surface attachment and a direct mechanism for electron uptake has been proposed, it is conceivable that *M. maripaludis* and other methanogens may be able to use appendages to shuttle electrons across conductive mineral surfaces when electron donors such as H<sub>2</sub> are scarce possibly through a cathodic depolarization mechanism. If this is the case, future research could focus on engineering this attribute to increase methanogenesis without the input of hydrogen which is both expensive and dangerous to work with on large scales.



### 3. MATERIALS AND METHODS

#### 3.1. Mineral Selection and Preparation

To capture the full range of electrical conductivity likely to be encountered in geologic formations, minerals were selected using the work of Palacky (1988).<sup>31</sup> In this study, earth materials were plotted as a function of electrical conductivity (Figure 1). For example, at the lower end of mineral electrical conductivity (herein referred to as,  $EC_{min}$ ) limestone chalk ( $\text{CaCO}_3$ ) and quartz ( $\text{SiO}_2$ ) were chosen with  $EC_{min}$  range of  $0.01\text{-}1 \text{ mS m}^{-1}$  and  $0.1\text{-}2 \text{ mS m}^{-1}$ , respectively. Kaolinite clay ( $\text{Al}_2\text{Si}_2\text{O}_5(\text{OH})_4$ ) served as the medium conductivity mineral with  $EC_{min}$  of  $10\text{-}200 \text{ mS m}^{-1}$ . Galena ( $\text{PbS}$ ), and pyrite ( $\text{FeS}_2$ ) were chosen as the high conductivity minerals found in reduced environments with  $EC_{min}$  of  $(1 \times 10^3 - 1 \times 10^5 \text{ mS m}^{-1})$ .

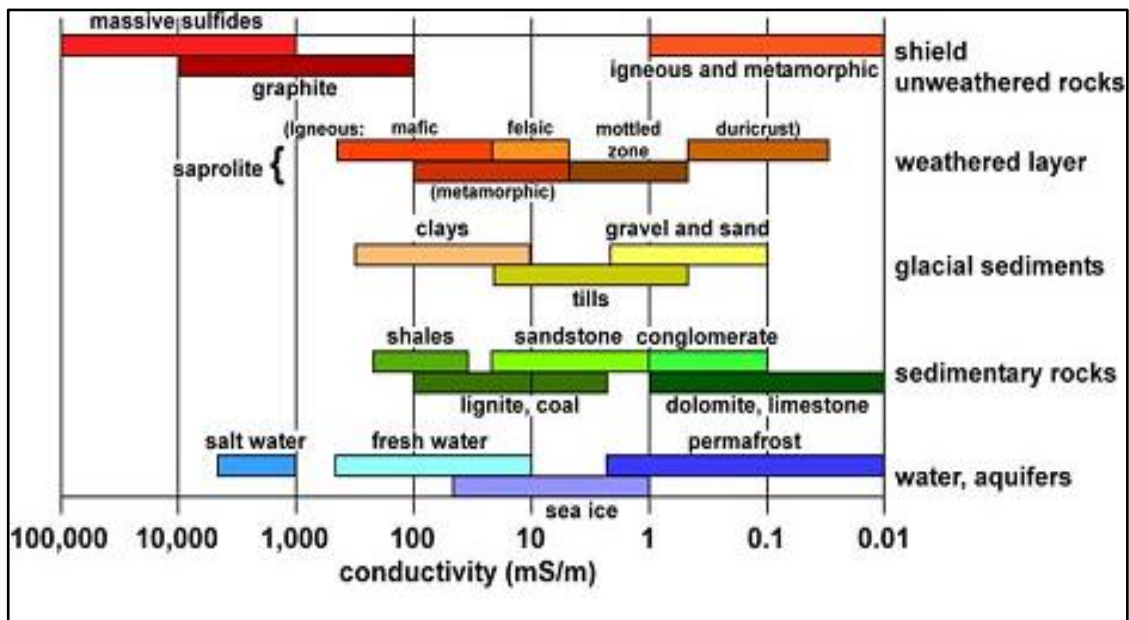


**Figure 1.** Electrical conductivity of rock units in  $\text{mS m}^{-1}$  with massive sulfide rock units (galena and pyrite) located at the high end of the conductivity scale while limestone, quartz (sand), and kaolinite are located at the lower range of conductivity.<sup>31</sup>

Limestone and kaolinite mineral surfaces were cleaned with lint-free wipes; quartz, galena and pyrite samples were cleaned with distilled H<sub>2</sub>O and dried with lint-free wipes. Samples were crushed separately using a mortar and pestle until fine enough to pass through a 500- $\mu$ m brass sieve. Galena and pyrite were subsequently cleaned with 0.5 M HCl and dried with N<sub>2</sub> gas in order to remove any oxides which may have been present on the mineral surface.

### **3.2. Sample Strain Cultivation**

Two strains of *M. maripaludis* were used; *Mm900* a wild-type/non-mutant strain and  $\Delta$ *flaB2* a non-archaeallated mutant strain (which lacks genes necessary for archaella). Both strains were acquired as gifts from Dr. Kenneth Jarrell in the Department of Biomedical and Molecular Sciences at Queen's University. Both strains were cultured in 250-mL serum bottles (VWR International Item # 10170-770; Chemglass Life Sciences # 4217-03) based on modified methods provided by Drs. William Whitman and Feng Long of the Department of Microbiology at the University of Georgia. Details of these methods are provided in Appendix A. In brief, two 50-mL batches of each strain were cultivated in a stationary 37°C incubator prior to each set of experiments. The growth media was deoxygenated by sparging with N<sub>2</sub> gas and placed in an anaerobic chamber where 45 mL were dispersed into 250-mL serum bottles. Reactors were then sealed and crimped in the anaerobic chamber and autoclaved on the gravity cycle at 121°C for 25 minutes. After cooling, 1 mL of Na<sub>2</sub>S·9H<sub>2</sub>O solution (25 g/L) was added to each of the four reactors followed by inoculation of two reactors with 5 mL of *Mm900*, and two with 5 mL of  $\Delta$ *flaB2*. Reactors were then pressurized with 80/20 v/v H<sub>2</sub>/CO<sub>2</sub> gas to a pressure of 200 kPa, shaken for 30 seconds, and moved to the

37°C incubator room. Each reactor was re-pressurized and shaken every 24-36 hours during the incubation period.

### **3.3. Assessment of mineral effects on CO<sub>2</sub>-to-CH<sub>4</sub> conversion by *M. maripaludis***

Two sets of experiments were conducted to assess mineral effects on CO<sub>2</sub>-to-CH<sub>4</sub> conversion. Both sets of experiments were conducted in crimp-style anaerobic glass reactors in the presence and absence of H<sub>2</sub> (referred to as H<sub>2</sub>-rich and H<sub>2</sub>-limited conditions, respectively) and with mutant and non-mutant *M. maripaludis*. Each experimental set consisted of the following treatments: Minerals of varying conductivity with inoculum, non-mineral reactors with inoculum, gas blank reactors with N<sub>2</sub> gas instead of H<sub>2</sub> for hydrogen-rich experiments (and vice versa), and media blanks with no inoculum; with each treatment conducted in triplicates.

Experimental set 1 was focused on identifying general growth trends with respect to mineral conductivity in H<sub>2</sub>-rich and H<sub>2</sub>-limited environments and included the full complement of minerals: limestone, quartz, kaolinite, pyrite, and galena. These experiments were carried out in 28 mL glass “Balch” tube reactors (VWR International #89167-180; Chemglass Life Sciences #4209-10) for incubation periods of 1 and 14 days. For mineral treatments, 0.5 ± 0.01 g of each mineral were added to the reactors in triplicates. The reactors (including those for gas and media blanks) were then covered and transferred into an anaerobic chamber (VAC 101965 OMNI-LAB) along with 1 L of freshly prepared growth medium. While in the anaerobic chamber, 4 mL of archaea growth medium was transferred to each reactor receiving *M. maripaludis* cultures and 5 mL to medium blanks which would receive no cultures. Reactors were then sealed and crimped with butyl rubber stoppers and aluminum seals. Stoppers and aluminum seals were acquired from VWR International (Item

# 30624-022 and 89167-1834) and Chemglass Life Sciences (item # 4209-14 and 4209-12). Crimped reactors were removed from the chamber, autoclaved (121°C on gravity setting for 25 minutes), cooled to room temperature, the top of each tube flame-sterilized and 0.1 mL of Na<sub>2</sub>S·9H<sub>2</sub>O solution injected into the reactors. Reactors were then shaken vigorously and allowed to sit at room temperature for a period of 18 hours.

After the 18h sitting period, mineral and non-mineral *M. maripaludis* treatments were inoculated with 1 mL of mutant or non-mutant strains. Reactors for H<sub>2</sub>-rich treatments were then flushed for 1 minute, pressurized to 200 kPa with H<sub>2</sub>/CO<sub>2</sub> gas mixture (certified 80% H<sub>2</sub> and 20% CO<sub>2</sub> mix) and incubated for 1 and 14 days at 37 °C. Reactors for H<sub>2</sub>-limited treatments, were treated similarly except instead of the 80% H<sub>2</sub> /20% CO<sub>2</sub> gas mix, an 80% N<sub>2</sub> /20% CO<sub>2</sub> gas mix was used for flushing and pressurizing the reactor headspace. pH measurements were taken on each sampling, but were not used in data analysis (Appendix B).

Experimental set 2 was focused on assessing kinetics of  $R_{CH_4}$  (CH<sub>4</sub>:CH<sub>4</sub>+CO<sub>2</sub>) across minerals under H<sub>2</sub>-rich and H<sub>2</sub>-limited conditions. These experiments were similar in many aspects to experimental set 1 except reactors were 250-mL glass serum bottles (rather than 28-mL Balch tubes used in experimental set 1) and sampling of headspace CH<sub>4</sub> and CO<sub>2</sub> was taken on day 1, 2, 3, and 4 (not just day 1 and 14). Experiment 2 also include only limestone and pyrite - minerals from both extremes of the electrical conductivity spectrum. In order to maintain the same mineral-to-solution ratio (~1:10) as in experimental set 1 mineral mass and volumes for archaea growth media, inoculum and Na<sub>2</sub>S·9H<sub>2</sub>O were increased by a factor of 10. Mineral treatments in experimental set 2 contained 5g of mineral, 45 mL of growth media, 5 mL inoculum and 1 mL of Na<sub>2</sub>S·9H<sub>2</sub>O solution. As in experimental set 1, reactors

were flushed and pressurized to 200 kPa with 80/20 gas mixture of H<sub>2</sub>/CO<sub>2</sub> (for H<sub>2</sub>-rich treatments) or N<sub>2</sub>/CO<sub>2</sub> (for H<sub>2</sub>limited treatments) and incubated at 37°C.



**Figure 2.** Experimental Setup in Anaerobic Chamber where media was transferred to “Balch” tubes with varying treatments followed by crimping and sealing.



**Figure 3.** Sealed and crimped reactors prior to autoclaving, inoculation, and pressurizing with H<sub>2</sub>/CO<sub>2</sub> or N<sub>2</sub>/CO<sub>2</sub> gas.



**Figure 4.** Incubation of reactors in a 37°C incubator room.

### **3.4 Headspace Gas Sampling and Analysis**

All headspace gas measurements were made using gas chromatography. The gas chromatograph used was a “greenhouse” gas GC (SRI 8610C) from SRI instruments. Sample introduction into the instrument was facilitated via a 10-port gas sampling valve with 1-mL sampling loop. Gas separation was via a 15’ HAYESEP-D column with N<sub>2</sub> as the carrier gas. For gas detection, the instrument was equipped with both an electron capture (ECD) and a flame ionization detector (FID). Operating conditions for the instrument during CO<sub>2</sub> and CH<sub>4</sub> analysis was 100 °C oven temperature and carrier flow was 30 psi nitrogen. Average elution time for CO<sub>2</sub> and CH<sub>4</sub> were 2.00 and 3.15 minutes respectively. Calibration curves for CO<sub>2</sub> and CH<sub>4</sub> were established daily using calibration gases containing 5 and 20% of CO<sub>2</sub> and CH<sub>4</sub>. Calibration gases were purchased from GASCO Gas Company and were run in triplicates.

To introduce the gas (calibration or headspace gas) sample into the sample loop, a 5 – mL syringe was connected to the outlet side of 10-port valve - with the sample to be tested connected to the inlet side. For the calibration gases, connection was directly through a tube from the valve of the calibration gas canister to the inlet of 10-port valve (Figure 5a). For headspace gas sampling, the reactors were connected to the inlet side of the 10-port via a flame-sterilized syringe needle plunged through the top of the flame-sterilized crimp seal and into the headspace (Figure 5b). The piston of the 5-mL syringe on the outlet end was then pulled from the 0 to 3 mL position, allowing for filling of 1-mL sample loop. Once the sample loop was filled, the valve was activated to the “inject” mode resulting in injection of the sample onto the 15’ HAYESEP-D column.

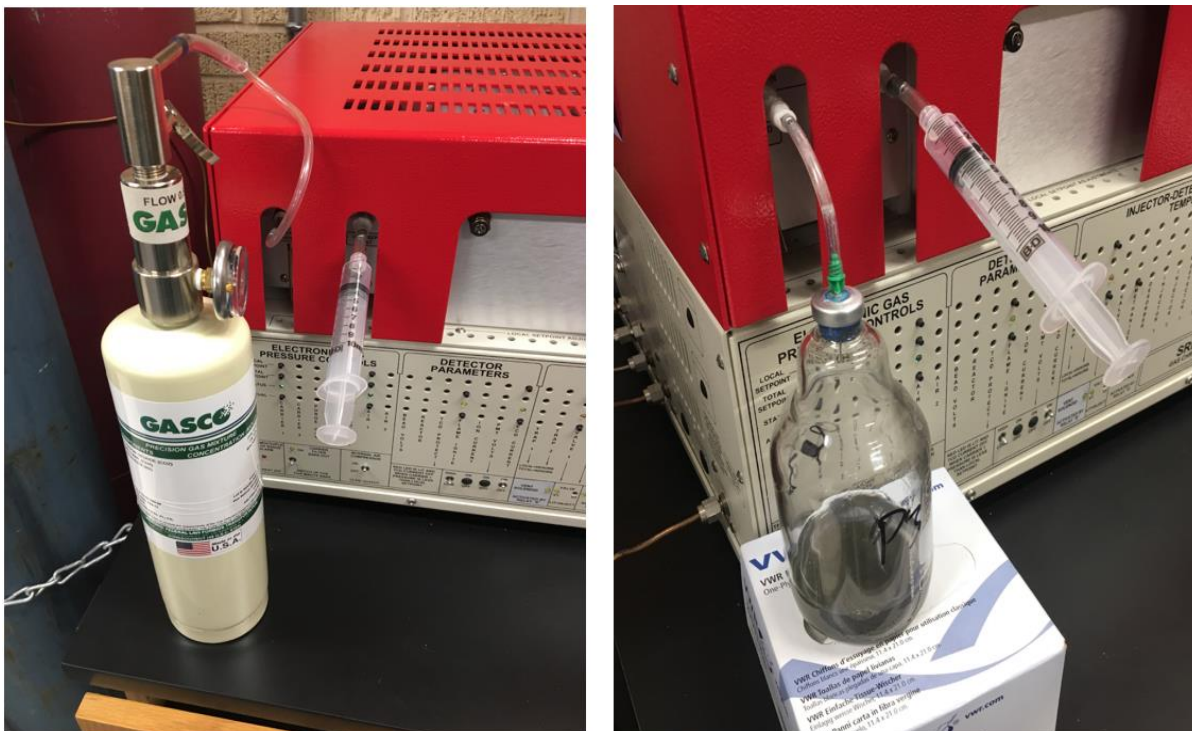


**Figure 5.** Gas chromatograph injection of a) gases drawn directly into GC with plastic syringe. b) reactor headspace drawn through vacutainer needle into the loop with syringe calibration.

Peaks for CO<sub>2</sub> and CH<sub>4</sub> on the resulting chromatographs were integrated and compared to those for calibration gases to determine CO<sub>2</sub> and CH<sub>4</sub> concentration, and the concentrations were used to calculate the relative CO<sub>2</sub>-to-CH<sub>4</sub> conversion ratio ( $R_{CH4}$ ) for each treatment. Relative CO<sub>2</sub>-to-CH<sub>4</sub> conversion ratio was calculated as:

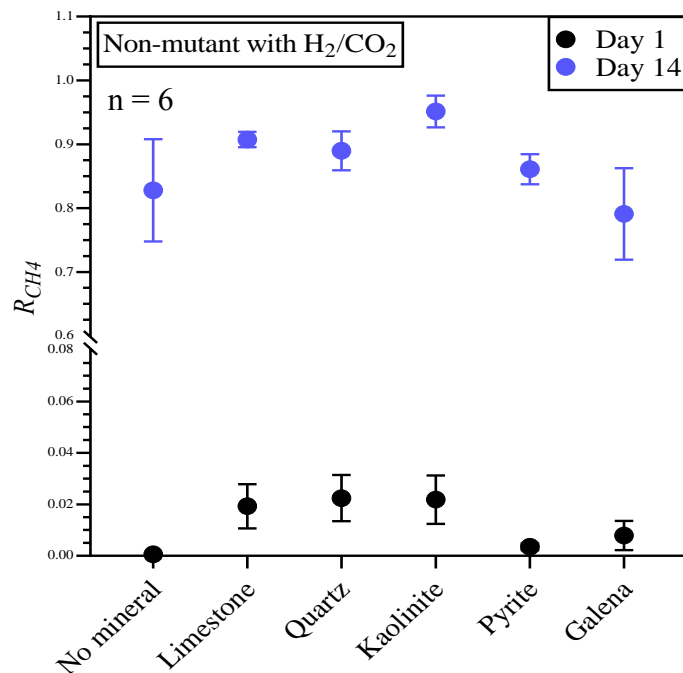
$$R_{CH4} = \frac{[CH_4]}{[CH_4] + [CO_2]}$$

where,  $[CH_4]$  and  $[CO_2]$  are the average concentrations of CO<sub>2</sub> and CH<sub>4</sub> respectively across triplicate reactors within a given experimental treatment. Overall concentrations of CH<sub>4</sub> and CO<sub>2</sub> were not used for these analyses, but are reported in Appendix C.

## 4. RESULTS

### 4.1. Mineral electrical conductivity ( $EC_{min}$ ) effects on CO<sub>2</sub>-to-CH<sub>4</sub> conversion ratio ( $R_{CH4}$ ) by *M. maripaludis*

#### 4.1.1 Insights on $EC_{min}$ - $R_{CH4}$ relationship from experiments in H<sub>2</sub>-rich environments



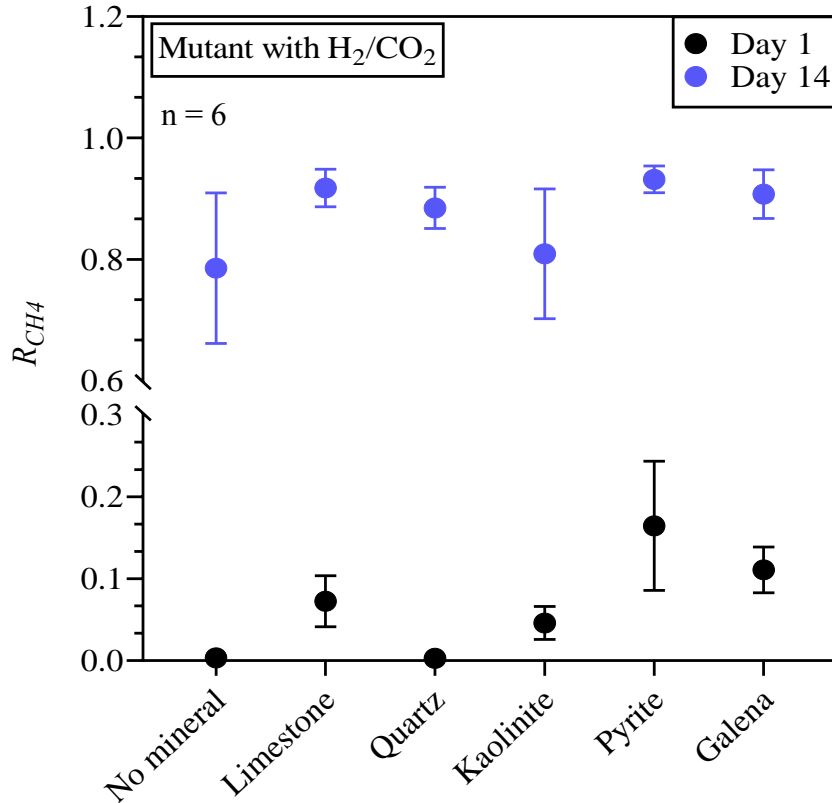
**Figure 6.**  $R_{CH4}$  for wild-type *Mm900* across varying mineral type in H<sub>2</sub>/CO<sub>2</sub> for 1 and 14 with days



Figure 6 shows the  $R_{CH_4}$  values in the reactor headspace for days 1 and 14 from experimental set 1 under H<sub>2</sub>-rich conditions. Minerals are arranged from left-to-right in order of increasing electrical conductivity. I.e. the average electrical conductivity for the minerals follow the order limestone < quartz < kaolinite (clay) < pyrite (sulfide) ≤ galena (sulfide). Figure 6 indicated that within the first day of incubation, there was no detectable quantity of CH<sub>4</sub> among the total carbon gas (CO<sub>2</sub>+ CH<sub>4</sub>) measured in the headspace of reactors containing no mineral and the high electrical sulfide minerals (galena or pyrite). This was consistent with an absence of CO<sub>2</sub>-to-CH<sub>4</sub> conversion by *Mm900* on day 1 under H<sub>2</sub>-rich condition in these treatments. In contrast, 2-3% ( $R_{CH_4} = 0.02 - 0.03$ ) of the total carbon gas in the low conductivity minerals (quartz, limestone and kaolinite) was CH<sub>4</sub> - suggesting that at least in the early stages of the experiment, CO<sub>2</sub>-to-CH<sub>4</sub> conversion by *Mm900* under H<sub>2</sub>-rich conditions was inversely related to mineral conductivity.

By day 14,  $R_{CH_4}$  in the non-mineral reactors increased to 0.89 (from 0 on day 1) in the reactor headspace and was comparable to that in the quartz-, limestone- and kaolinite-containing reactors – with  $R_{CH_4}$  of 0.89, 0.91 and 0.95, respectively (Figure 6). Galena- and pyrite-containing reactors had significantly lower  $R_{CH_4}$  (0.79 and 0.86, respectively) – consistent with the qualitative trends observed on day 1. The fact that the qualitative trend in the mineral conductivity- $R_{CH_4}$  relationship from day 1 and day 14 was similar throughout the experiment (i.e. lower electrical conductivity of minerals favors higher  $R_{CH_4}$ ) suggested that, under H<sub>2</sub>-rich conditions, CO<sub>2</sub>-to-CH<sub>4</sub> conversion in the *Mm900* strain was being enhanced in the presence of lower versus higher conductivity mineral in H<sub>2</sub>-rich environments. It is also worth noting that average concentrations of CH<sub>4</sub> produced by *Mm900* in the headspace of H<sub>2</sub>-rich reactors were congruent with this trend. For example, on day 14 the reactors

containing limestone, quartz and kaolinite, averaged 4-7% CH<sub>4</sub> compared to 1-3% in pyrite- and galena-bearing reactors.



**Figure 7.**  $R_{CH_4}$  for non-archaellated  $\Delta flaB2$  with varying mineral type in H<sub>2</sub>/CO<sub>2</sub> for day 1 and 14

Very different mineral- $R_{CH_4}$  relationships were apparent in H<sub>2</sub>-rich conditions for the non-archaellated  $\Delta flaB2$  than was observed for the archaellated *Mm900* strain. In contrast to the inverse relationship observed between mineral conductivity and  $R_{CH_4}$  for *Mm900* (Figure 6), for  $\Delta flaB2$ ,  $R_{CH_4}$  on day 1 was generally lower ( $R_{CH_4} = 0-0.07$ ) in reactors containing the low-conductivity minerals (limestone, quartz and kaolinite) than in those containing the high conductivity minerals (pyrite and galena;  $R_{CH_4} = 0.11-0.17$ ). No clear trend between mineral conductivity and  $R_{CH_4}$  was apparent in the day 14 data for  $\Delta flaB2$  (Figure 7) suggesting that the positive mineral conductivity- $R_{CH_4}$  relationship observed on day 1 could (at least

qualitatively) be linked to enhancing effects of mineral conductivity on the early stages of CO<sub>2</sub>-to-CH<sub>4</sub> conversion by  $\Delta flaB2$  under H<sub>2</sub>-rich conditions.

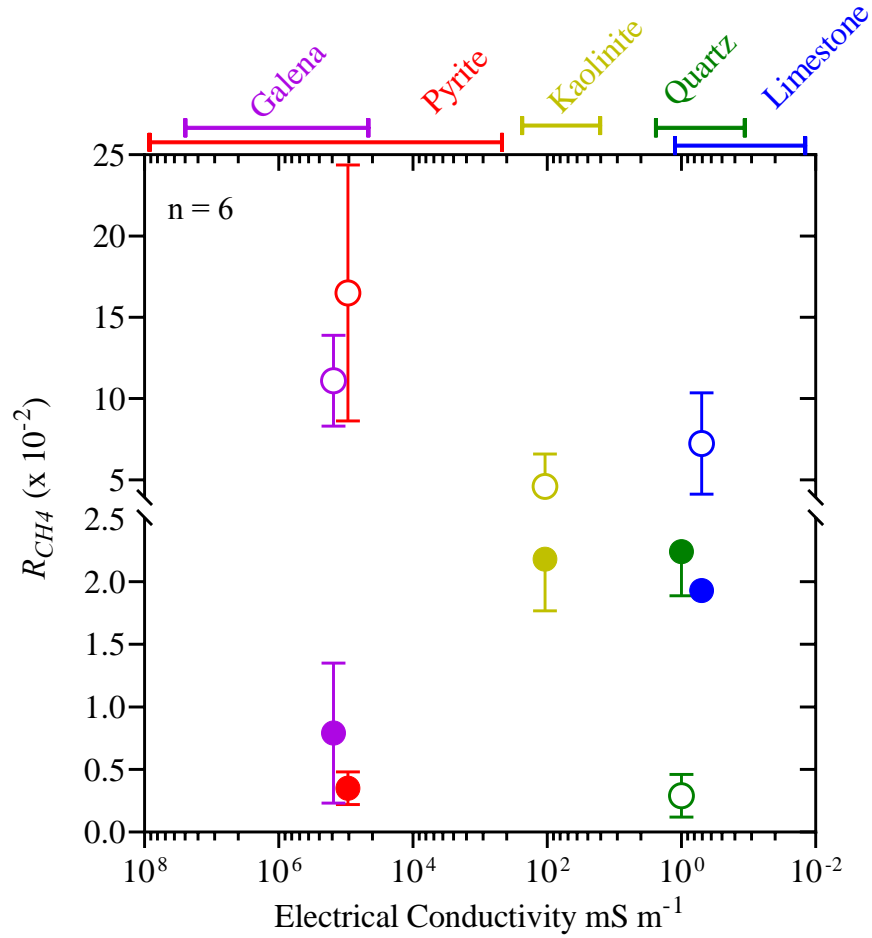


**Figure 8.** CO<sub>2</sub>-to-CH<sub>4</sub> conversion ratio ( $R_{CH_4}$ ) by *Mm900* (filled circles) and  $\Delta flaB2$  (open circles) as a function of mineral electrical conductivity on day 1 in H<sub>2</sub>-rich conditions.

Plotting  $R_{CH_4}$  (for *Mm900* and  $\Delta flaB2$ ) as a function of median  $EC_{min}$  on the same log-scale as Figure 1 suggested that effects on  $R_{CH_4}$  was linearly related to the log-transformed  $EC_{min}$  (Figure 8). That is, the  $R_{CH_4}$ - $EC_{min}$  relationship for *Mm900* and  $\Delta flaB2$  in H<sub>2</sub>-rich conditions could be described by the general equation:  $R_{CH_4} = m \log(EC_{min}) + c$ ; where the slope,  $m$ , of relationship indicates the direction and magnitude of the  $EC_{min}$  effects while the

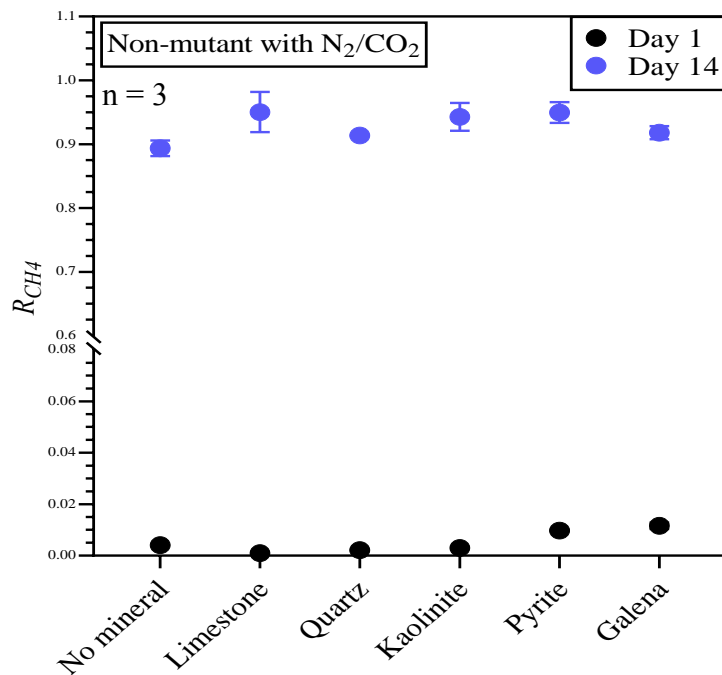
intercept,  $c$ , corresponds to the  $R_{CH_4}$  value expected in the presence of a mineral with  $EC_{min}$  of unit conductivity units (in this case,  $1 \text{ mS m}^{-1}$ ). Table 1 shows the  $R_{CH_4}$ - $\log(EC_{min})$  relationships for the minerals studied. For calcite, quartz and kaolinite the values used for median  $EC_{min}$  (0.5, 1, and  $100 \text{ mS m}^{-1}$ , respectively) were obtained from ranges for limestone, sand and clay in Figure 1. Median  $EC_{min}$  values for galena ( $1.5 \times 10^5 \text{ mS m}^{-1}$ ) and pyrite ( $9.3 \times 10^4 \text{ mS m}^{-1}$ ), were calculated from the range of resistivity measurements presented by Pridmore and Shuey (1976) for these minerals.<sup>32</sup>

Table 1 shows the  $R_{CH_4}$ - $\log(EC_{min})$  equations for day 1 and day 14  $\text{CO}_2$ -to- $\text{CH}_4$  conversion by *Mm900* and  $\Delta$ *flaB2* under  $\text{H}_2$ -rich conditions. These relationships confirmed the potential quantitative links between  $EC_{min}$  and the conversion of  $\text{CO}_2$  to  $\text{CH}_4$  by *Mm900* and  $\Delta$ *flaB2* under  $\text{H}_2$ -rich conditions. The day 1 values for *Mm900* showed a statistically significant ( $p$ -value = 0.032) non-zero slope with the equation of  $R_{CH_4} = -(2.99 \times 10^{-3})(\log(EC_{min})) + 0.022$  ( $R^2 = 0.829$ ). This indicates that under  $\text{H}_2$ -rich conditions *Mm900* exhibited significantly different trends in presence of minerals. The  $R_{CH_4}$ - $\log(EC_{min})$  relationships for day 14 did not show significant non-zero slopes (and therefore was not discussed in this paper). The values for  $\Delta$ *flaB2* in  $\text{H}_2$ -rich conditions did not show significance in either day of the experiment (1 or 14).

**Table 1.** Day 1 equations and fits for  $R_{CH_4}$ - $\log(EC_{min})$  relationships for  $Mm900$  and  $\Delta flaB2$  in  $H_2$ -rich and  $H_2$ -limited environments.

<b>Equations for <math>R_{CH_4}</math>-<math>\log(EC_{min})</math> Relationships</b>			
<b><u><math>H_2</math>-rich conditions (day 1)</u></b>	$m \log(EC_{min}) + c$	$p$ -value ( $m \neq 0$ )	$R^2$
<u><math>Mm900</math></u>	$-2.99 \times 10^{-3} \log(EC_{min}) + 0.022$	0.032	0.829
<u><math>\Delta flaB2</math></u>	$1.91 \times 10^{-2} * \log(EC_{min}) + 0.035$	0.092	0.666
<b><u><math>H_2</math>-limited conditions (day 14)</u></b>			
<u><math>Mm900</math></u>	$1.60 \times 10^{-2} * \log(EC_{min}) + 0.917$	0.182	0.500
<u><math>\Delta flaB2</math></u>	$5.47 \times 10^{-3} * \log(EC_{min}) + 0.038$	0.626	0.089

**4.1.2. Insights on  $EC_{min}$ - $R_{CH_4}$  relationship from experiments in  $H_2$ -limited environments**



**Figure 9.**  $R_{CH_4}$  for wild-type  $Mm900$  with varying mineral type in  $N_2/CO_2$  for days 1 and 14.

Figure 9 shows the  $R_{CH_4}$  values for day 1 and 14 for *Mm900* in H<sub>2</sub>-limited environments. Under these conditions, no mineral and lower-conductivity reactors showed low  $R_{CH_4}$  values ranging from 0.00-0.04. Galena and pyrite reactors produced significantly higher  $R_{CH_4}$  ratios during this period with 0.11 and 0.10, respectively. High-conductivity minerals produced significantly higher  $R_{CH_4}$  values during this time period compared with reactors with no minerals or minerals of lower conductivity. This was opposite of the day 1 trend seen in H<sub>2</sub>-rich *Mm900* reactors with a trend directly related to mineral conductivity (i.e. higher EC = higher  $R_{CH_4}$ ). By day 14, in non-mineral reactors CH<sub>4</sub> accounted for 0.89 of gaseous carbon which was comparable to mineral-containing reactors with quartz-, limestone-, kaolinite-, galena-, and pyrite-containing reactors having  $R_{CH_4}$  values ranging from 0.91 to 0.95 with no trend relative to mineral conductivity. With the exception of quartz, the highest final CH<sub>4</sub> concentration under H<sub>2</sub>-limited conditions with wild-type *Mm900* was congruent with the trend in  $R_{CH_4}$ . Reactors containing galena had day 14 CH<sub>4</sub> concentrations of (22.73%) followed by quartz (20.88%), pyrite (19.39%), kaolinite (18.30%), non-mineral (16.83%) and limestone (12.94%).

On day 1, the ratio of gaseous carbon as CH<sub>4</sub> for hydrogen-limited reactors containing mutant strain  $\Delta flaB2$  and no minerals was 0.01 which was comparable to limestone (0.00) and kaolinite reactors (0.01) as seen in Figure 10. Quartz reactors produced a relatively high  $R_{CH_4}$  value under these conditions with 0.13. In general,  $R_{CH_4}$  was higher in reactors containing minerals with higher conductivity ( $R_{CH_4}$  for galena and pyrite was 0.07 and 0.54, respectively) on day 1. By day 14, CH<sub>4</sub> represented 92-95% ( $R_{CH_4} = 0.92-0.95$ ) of all gaseous carbon in the headspace of the reactors showing no trend with mineral conductivity. Final overall CH<sub>4</sub> concentrations for non-archaeallated  $\Delta flaB2$  were highest in reactors

containing limestone (22.54%) followed by kaolinite (19.28%), non-mineral (18.90%), pyrite (15.34%), galena (14.13%), and quartz (9.23%).

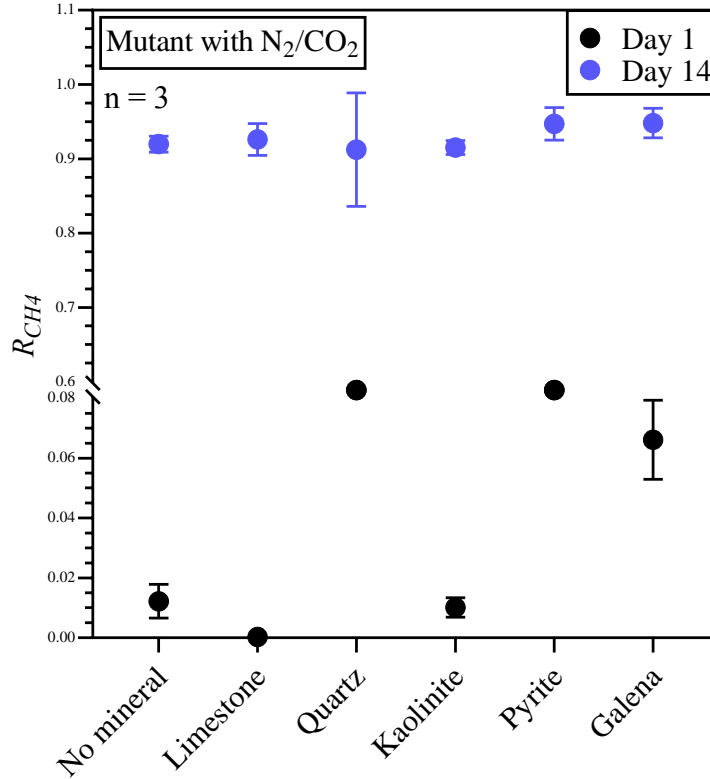


**Figure 10.**  $R_{CH_4}$  for non-archaeallated  $\Delta flaB2$  with varying mineral type in  $N_2/CO_2$  for days 1 and 14.

As with  $H_2$ -rich environments,  $R_{CH_4}$  values (for *Mm900* and  $\Delta flaB2$ ) showed linear relationships when plotted as a function of median  $EC_{min}$  on a log scale (Figure 11). Table 2 shows  $R_{CH_4}$ -log( $EC_{min}$ ) relationships and respective equations for day 1  $CO_2$ -to- $CH_4$  conversion by *Mm900* and  $\Delta flaB2$  under  $H_2$ -limited conditions. Day 1 relationships for *Mm900* showed a significant ( $p$ -value = 0.003) non-zero slope with the equation of  $R_{CH_4} = (1.80 \times 10^{-3})(\log(EC_{min})) + 0.001$  ( $R^2 = 0.961$ ). This indicates that under  $H_2$ -limited conditions *Mm900* exhibited significantly different trends in presence of minerals (which was also the case with *Mm900* in  $H_2$ -rich conditions). Again, the  $R_{CH_4}$  relationships for day 14

did not show significant non-zero slopes and therefore were discussed in this paper. The plots for  $\Delta flaB2$  in  $H_2$ -limited conditions once again showed no significance in either day of the experiment (1 or 14).

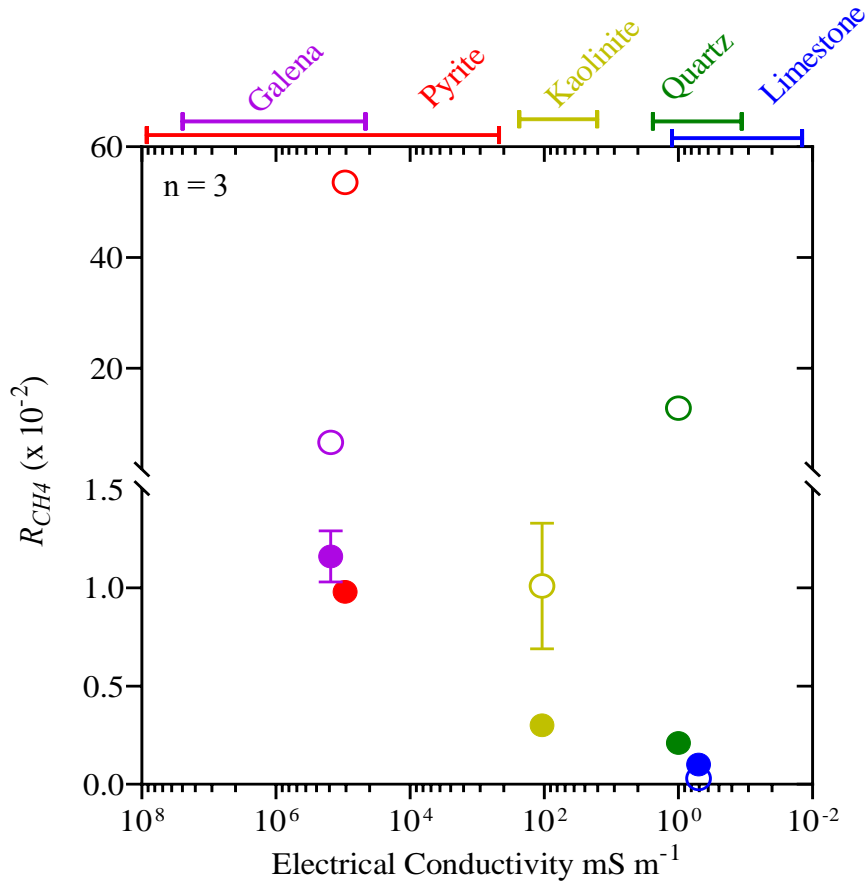


**Figure 11.** CO<sub>2</sub>-to-CH<sub>4</sub> conversion ratio ( $R_{CH4}$ ) by *Mm900* (filled circles) and  $\Delta flaB2$  (open circles) as a function of mineral electrical conductivity on day 1 in  $H_2$ -limited conditions.



**Table 2.** Day 14 equations and fits for  $R_{CH_4}$ -log ( $EC_{min}$ ) relationships for *Mm900* and  $\Delta flaB2$  in H<sub>2</sub>-rich and H<sub>2</sub>-limited environments.

<b>Equations for <math>R_{CH_4}</math>-log (<math>EC_{min}</math>) Relationships</b>			
<b><u>H<sub>2</sub>-rich conditions (day 1)</u></b>	<b><math>m \log(EC_{min}) + c</math></b>	<b><math>p</math>-value (<math>m \neq 0</math>)</b>	<b>R<sup>2</sup></b>
<i>Mm900</i>	$1.80 \times 10^{-3} \log(EC_{min}) + 0.001$	0.003	0.961
$\Delta flaB2$	$4.75 \times 10^{-2} * \log(EC_{min}) + 0.038$	0.323	0.317
<b><u>H<sub>2</sub>-limited conditions (day 14)</u></b>			
<i>Mm900</i>	$2.09 \times 10^{-4} * \log(EC_{min}) + 0.935$	0.182	0.500
$\Delta flaB2$	$5.65 \times 10^{-3} * \log(EC_{min}) + 0.917$	0.052	0.766

#### 4.1.3 Summary of general trend analysis for Experiment 1

Qualitative trends for experiment 1 revealed that in most (3/4) conditions reactors containing high-conductivity minerals outperformed non-mineral and low-conductivity reactors with respect to  $R_{CH_4}$  values. However, only day 1 values for reactors containing *Mm900* showed significant non-zero slope differentiation for these plots. Under H<sub>2</sub>-rich conditions, CO<sub>2</sub>-to-CH<sub>4</sub> conversion by *Mm900* exhibited a trend inversely related to mineral conductivity with low-conductivity minerals (limestone, quartz, and kaolinite) enhancing methanogenesis in early-stages (day 1). In contrast, under H<sub>2</sub>-limiting conditions this trend in  $R_{CH_4}$  was reversed with high-conductivity minerals (pyrite and galena) enhancing early-stage methanogenesis. This reversal of trends suggests that in the presence of hydrogen, electrons may preferentially be used for growth (not measured in these experiments) instead

of maintenance. In contrast, the H<sub>2</sub>-limited trend suggests that in the absence of hydrogen, conductive minerals may act as electron donors in the early-stages possible via cathodic depolarization as reported in elemental metals.<sup>33</sup>

An increase in early-stage methanogenesis involving mutant strain  $\Delta flaB2$  was seen in reactors containing galena and pyrite in both hydrogen-rich and hydrogen-limited reactors (as well as non-mutant H<sub>2</sub>-limited reactors). This result would not be expected if archaeella are involved in the direct uptake mechanism established by Lohner *et al.*<sup>15</sup> or any indirect mechanism involving electron shuttling by *M. maripaludis*.<sup>21</sup> However, non-zero slopes for  $R_{CH_4}$ -log (EC<sub>min</sub>) relationships in  $\Delta flaB2$  reactors were not significant showing that qualitative trends seen in non-archaeellated reactors were not significantly different than non-mineral controls.

#### **4.2. Mineral effects on kinetics of CO<sub>2</sub>-to-CH<sub>4</sub> conversion**

Results from Experimental set 1 highlighted several important aspects of mineral effects on conversion of CO<sub>2</sub>-to-CH<sub>4</sub> in H<sub>2</sub>-rich and H<sub>2</sub>-limited environments. For example, early-stage methanogenesis was found to be significantly impacted by mineral type in H<sub>2</sub>-rich environments, but not in H<sub>2</sub>-limited environments. In addition, these significant trends were opposing with respect to mineral conductivity with limestone reactors having higher  $R_{CH_4}$  values than pyrite under H<sub>2</sub>-rich conditions (and vice versa- under H<sub>2</sub>-limited conditions). One observation of primary importance is the fact that any differences across mineral treatments were significant in day 1 (but not in day 14) - suggesting that mineral effects were most likely kinetically driven. Data from experimental set 2 were used to assess mineral effects on the kinetics of CO<sub>2</sub>-to-CH<sub>4</sub> conversion by *Mm900* and  $\Delta flaB2$  in both H<sub>2</sub>-rich and H<sub>2</sub>-limited conditions. Experiments included non-mineral, limestone- and pyrite-

containing treatments. Limestone and pyrite were used to represent the lower and higher end of the mineral conductivity spectrum, respectively. The much larger volume of the 250-mL reactors (compared to 28 mL in Experimental set 1) used in these experiments allowed for 1) a significant reduction in the number of reactors needed and 2) multiple sampling of each headspace-thereby reducing intra-experiment variability associated with sampling.

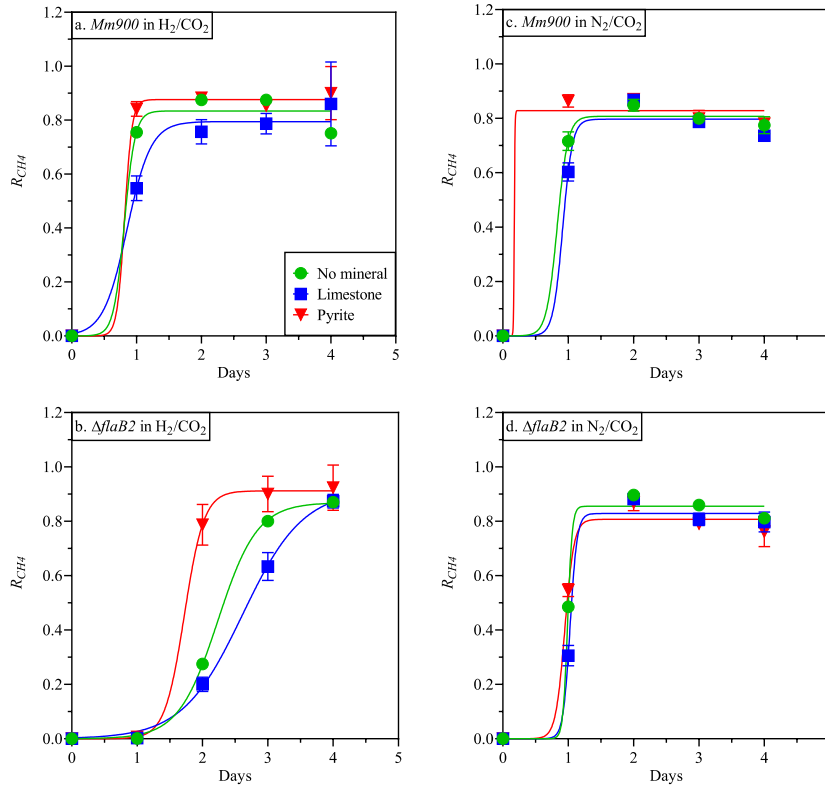
#### **4.2.1. Temporal trends and kinetics of CO<sub>2</sub>-to-CH<sub>4</sub> conversion**

Figure 12 shows the temporal evolution in  $R_{CH_4}$  for *Mm900* and  $\Delta$ *flaB2* in non-mineral, limestone- and pyrite-containing reactors under both H<sub>2</sub>-rich conditions and H<sub>2</sub>-limited conditions. In all cases,  $R_{CH_4}$  peaked and leveled off within 4 days of initiation - indicating that CO<sub>2</sub>-to-CH<sub>4</sub> conversion was completed within 4 days. Peak  $R_{CH_4}$  were always between 0.80 and 0.90, congruent with those observed in experimental set 1 and further confirmed that observed differences were dictated by differences in CO<sub>2</sub>-to-CH<sub>4</sub> conversion kinetics. Time to peak  $R_{CH_4}$  across treatments followed the general order limestone > non-mineral > pyrite. In contrast, trends in day-1  $R_{CH_4}$  followed the order pyrite > non-mineral > limestone consistent with the overall rate of CO<sub>2</sub>-to-CH<sub>4</sub> conversion being highest in pyrite-containing and lowest in limestone-containing reactors.

A logistic (sigmoidal) model was used to estimate key kinetic parameters for CO<sub>2</sub>-to-CH<sub>4</sub> conversion mediated by *Mm900* and  $\Delta$ *flaB2* in the presence/absence of limestone/pyrite under H<sub>2</sub>-rich and H<sub>2</sub>-limited conditions. The model was fitting using Graphpad Prism© software and was of the form:

$$R_{CH_4} = \frac{c}{1 + e^{-k(t-t_{1/2})}}$$

where  $R_{CH4}$  is the conversion ratio for CO<sub>2</sub> to CH<sub>4</sub>;  $c$  is the maximum conversion captured by the model;  $k$  is the pseudo-first order rate constant in units of day<sup>-1</sup>;  $t$  is the experimental time/length of incubation in units of days;  $t_{1/2}$  is the time corresponding to half of  $R_{CH4}$  captured by the experiment/model.



**Figure 12.** Kinetics of CO<sub>2</sub>-to-CH<sub>4</sub> conversion ( $R_{CH4}$ ) in H<sub>2</sub>-rich and H<sub>2</sub>-limited environments with wild-type *Mm900* and non-archaeallated  $\Delta flaB2$  with respect to non-mineral(green), limestone (blue) and pyrite (red).

Model fits to the  $R_{CH4}$  versus time data reflected good fits for all scenarios plotted (Figure 12). Values for co-efficient of determination,  $R^2$  ranged between 0.966 and 0.999 indicating that the model captured 97-99% of variability in  $R_{CH4}$  with time (Table 2). Table 2 also summarizes the fitted parameters for the model. That is,  $c$ ,  $k$  and  $t_{1/2}$ .

**Table 3.** Modeled parameters max conversion (c), rate constant (k), and half-life ( $t_{1/2}$ ) with  $r^2$  values. Standard error has been reported where applicable.

<b>Modeled Parameters</b>				
<b><u>H<sub>2</sub>-rich conditions</u></b>	<i>c</i>	<i>Rate constant, k</i>	<i>t<sub>1/2</sub></i>	<b>R<sup>2</sup></b>
<u><i>Mm900</i></u>				
<i>No Mineral</i>	0.834 ± 0.021	12.0	0.811	0.986
<i>Limestone</i>	0.795 ± 0.024	5.43	0.854 ± 0.138	0.966
<i>Pyrite</i>	0.876 ± 0.013	17.3	0.815	0.991
<u><i>ΔflaB2</i></u>				
<i>No Mineral</i>	0.869 ± 0.008	3.32 ± 0.172	2.24 ± 0.018	0.999
<i>Limestone</i>	0.915 ± 0.026	2.17 ± 0.162	2.62 ± 0.049	0.995
<i>Pyrite</i>	0.912 ± 0.022	6.66	1.72 ± 0.181	0.988
<b><u>H<sub>2</sub>-limited conditions</u></b>				
<u><i>Mm900</i></u>				
<i>No Mineral</i>	0.808 ± 0.012	12.3	0.832	0.991
<i>Limestone</i>	0.797 ± 0.017	13.6	0.917	0.98
<i>Pyrite</i>	0.829 ± 0.013	181	0.175	0.987
<u><i>ΔflaB2</i></u>				
<i>No Mineral</i>	0.855 ± 0.011	28.5	0.991	0.993
<i>Limestone</i>	0.829 ± 0.016	18.7	1.03	0.989
<i>Pyrite</i>	0.807 ± 0.016	14.3	0.948	0.982

In H<sub>2</sub>-rich environments containing wild-type *Mm900*, the highest *c* value was found in reactors containing pyrite ( $0.876 \pm 0.013$ ) followed by reactors containing no minerals ( $0.834 \pm 0.021$ ) and limestone ( $0.795 \pm 0.024$ ). In similar environments containing non-archaeallated  $\Delta flaB2$ , pyrite reactors produced slightly lower *c* values than limestone with  $0.912 \pm 0.022$  and  $0.915 \pm 0.026$ , respectively. Reactors with no minerals had the lowest *c* values under these conditions with  $0.869 \pm 0.010$ . The trends in H<sub>2</sub>-rich environments do not match across archaeallated and non-archaeallated treatments. In H<sub>2</sub>-limited environments containing wild-type *Mm900*, the highest *c* value was found in reactors containing pyrite once again ( $0.829 \pm 0.013$ ) which was slightly higher than both non-mineral ( $0.808 \pm 0.012$ ) and limestone ( $0.797 \pm 0.017$ ) reactors. H<sub>2</sub>-limited reactors containing  $\Delta flaB2$  and pyrite produced the lowest *c* values ( $0.807 \pm 0.016$ ). Non-mineral reactors produced the highest values under these conditions ( $0.855 \pm 0.011$ ) followed closely by limestone ( $0.829 \pm 0.016$ ). In both environments, wild-type *M. maripaludis* produced the highest maximum conversion following a trend in reactor mineral conductivity; pyrite>non-mineral>limestone. Conversely, pyrite reactors containing  $\Delta flaB2$  produced slightly lower *c* values than limestone reactors in both H<sub>2</sub>-rich and H<sub>2</sub>-limited environments.

The rate constant (*k*) for wild-type *Mm900* in H<sub>2</sub>-rich environments was highest in pyrite reactors (~17.3) and followed the same trend that was seen in the *c* values. Non-mineral reactors had the second highest *k* values (~12.0), followed by reactors with limestone (5.43). Unlike the opposing trends seen with *c* values (with respect to *Mm900*), *k*-value trends for  $\Delta flaB2$  in H<sub>2</sub>-rich environments were similar to those seen in the wild-type strain; pyrite>non-mineral>limestone. Reactors containing pyrite had the highest rate constant (6.66) followed by non-mineral ( $3.32 \pm 0.17$ ) and limestone ( $2.17 \pm 0.16$ ) reactors. In H<sub>2</sub>-

limited environments,  $k$  values for wild-type *M. maripaludis* in reactors containing pyrite were unrealistic. However, non-mineral and limestone reactors exhibited trends opposite those seen in H<sub>2</sub>-rich environments (Limestone>non-mineral). The rate constant for limestone reactors was ~13.56 which was slightly higher than non-mineral reactors (~12.25) under these conditions.  $k$  values for reactors with  $\Delta flaB2$  were highest in reactors with no minerals (~28.53) followed by limestone and pyrite reactors at ~18.72 and ~14.27, respectively. No trend between rate constant and mineral conductivity could be determined under these conditions.

The half-life parameter ( $t_{1/2}$ ) is slightly different than the other two parameters in that the lower value corresponds to the fastest time. This is the amount of time in days that it takes for 50% conversion of CO<sub>2</sub> to CH<sub>4</sub> in each reactor. The fastest half-life in H<sub>2</sub>-rich reactors containing *Mm900* was seen in the absence of minerals (~0.811 days) followed by reactors containing pyrite (~0.815 days) and limestone (0.854), respectively. In reactors containing  $\Delta flaB2$ , those containing pyrite had the fastest half-life ( $1.724 \pm 0.18$  days) followed by non-mineral reactors ( $2.236 \pm 0.02$  days) and limestone reactors ( $2.616 \pm 0.05$ ). In H<sub>2</sub>-limited conditions, half-life values for reactors containing *Mm900* and pyrite were unrealistic and therefore were not plotted. Non-mineral reactors had the shortest half-life at ~0.832 days while limestone reactors were slightly slower during the experiment (~0.917 days). Under H<sub>2</sub>-limited conditions, reactors containing  $\Delta flaB2$  had the shortest half-life in the presence of pyrite (~0.948 days) followed closely by non-mineral (~0.991 days) and limestone (~1.029 days) reactors. In all mineral reactors,  $t_{1/2}$  was shortest in the presence of pyrite (with the exception of *Mm900* H<sub>2</sub>-limited) and lowest with limestone. However, non-mineral reactors had the shortest half-life in mutant reactors under both conditions.

## CONCLUDING REMARKS

The majority (7/8) of reactors sampled in our experiment saw increases in early-stage methanogenesis in the presence of high-conductivity minerals. Inhibition of  $\text{SO}_4^{2-}$ -respiring bacteria (as seen in syntrophic communities) can be ruled out as the mechanism for increased methanogenesis because only *M. maripaludis* was present in each treatment.<sup>14</sup> Although debated frequently, a mechanism involving cathodic depolarization seems the most likely to be causing increases in methanogenesis in the presence of high-conductivity minerals.<sup>15</sup> Most reactors showed increases in  $\text{CO}_2$ -to- $\text{CH}_4$  conversion in the presence of these minerals, but it is the  $\text{H}_2$ -limited treatments that are the most interesting. The fact that reactors saw similar trends with increasing conductivity in these environments suggests that enhancement is derived from the minerals irrespective of the presence of  $\text{H}_2$  which fits with cathodic depolarization theory. Limestone, quartz, and kaolinite (low-, med-conductivity) are not made of redox active metal ions like those seen in pyrite and galena, so the trends seen through these experiments are plausible if cathodic depolarization is occurring. Future studies should focus on these mineral/methanogen interactions, and also the interactions between minerals and varying environments in the absence of methanogens. Although unlikely to occur in the highly reduced conditions typically found in subsurface environments, it is possible some of the reducing agents in the growth medium are responsible for this observed reduction despite the stable configuration of these metals commonly found in the subsurface.

The quantitative trends plotted on  $R_{\text{CH}_4}$ - $\log(\text{EC}_{\text{min}})$  in experiment 1 showed significant opposing trends in early-stage methanogenesis in *Mm900* reactors when subjected to different environments;  $\text{H}_2$ -rich had higher  $R_{\text{CH}_4}$  ratios in reactors with low-conductivity



while in H<sub>2</sub>-limited reactors ratios were highest in reactors containing high-conductivity minerals. While it is not certain why these trends differ in these environments, the fact that only archaeallated specimens showed significant trends in the early stages of methanogenesis may be important. Although this evidence was indirect, it suggested that minerals only make a difference when archaeella are present during the early-stages methanogenesis. However, in experiment 2, pyrite was shown to enhance both  $k$  and  $t_{1/2}$  with mutant reactors in H<sub>2</sub>-rich conditions. Therefore, it is more likely that if electron shuttling is occurring it is happening in the cell structure with archaeella facilitating attachment to mineral surfaces.

Although all of the kinetic parameters ( $c$ ,  $k$ ,  $t_{1/2}$ ) plotted in experiment 2 had significant R<sup>2</sup>-values, only  $c$  provided consistent standard errors for the model. Since both  $k$  and  $t_{1/2}$  are temporal parameters, it is likely that 4 days was too long of a duration for modeling the kinetics associated with these reactions. Higher resolution sampling at times below 1-day would likely improve the tightness of the error bars associated with the estimates for these parameters. The  $c$  values in pyrite reactors containing *Mm900* were higher than limestone in both H<sub>2</sub>-rich and H<sub>2</sub>-limited environments as opposed to mutant strain  $\Delta flaB2$  (limestone > pyrite in both environments). As opposed to the trends seen in experiment 1,  $c$  values for archaeallated strains were enhanced in the presence of pyrite in both environments. This would be expected if archaeella are directly involved in electron shuttling. However, in mutant reactors no trend would be expected with respect to respect to mineral conductivity instead of limestone outperforming pyrite. Therefore, from the evidence given it is likely that archaeella are not used in direct electron shuttling, but as a means of motility and attachment to mineral surfaces.

## Appendix A: Detailed Growth Media Preparation

### Basal medium for formate growth (McF) of *Methanococcus maripaludis*

Modified from Feng Long, Whitman Lab, University of Georgia

1. Select appropriate glassware for experiment. For cultivation, 250-mL anaerobic bottles (Chemglass CLS-4217-03) were used to ensure enough headspace for 50 mL of inoculum.
2. Medium Composition:

Component	For 1 liter bottle
Glass-distilled water	500ml
General salts solution	500ml
K <sub>2</sub> HPO <sub>4</sub> , 14g/L	10ml
Na acetate·3H <sub>2</sub> O, 136 g/L	10ml
Trace mineral solution	10ml
Iron stock solution	5ml
Rezasurin, 0.1g/100ml	1ml
Sodium formate (NaCOOH)	27g
Sodium bicarbonate (NaHCO <sub>3</sub> )	5.0g

Combine medium ingredients in a 1-L flask and sparge with a stream of N<sub>2</sub> gas for 60 minutes.

3. Add 0.05g cysteine-HCl per 100ml and continue sparging until clear.

4. Transfer medium in anaerobic chamber, dispense 45 mL of medium into each culture vessel and seal tubes with blue butyl rubber stopper and aluminum crimp seal (VWR International# 98167-180, 30624-022, and 89167-184)
5. After removing from the anaerobic chamber, autoclave on gravity cycle for 25 minutes.
6. Prior to inoculation, flame sterilize and add 1 ml of 2.5% Na<sub>2</sub>S·9H<sub>2</sub>O (w/v) per 50 ml of medium.
7. Flame-sterilize once again and inoculate culture vessels with 5 mL of inoculum per 50 mL vessel.
8. Using a syringe-filter and an exhaust needle, cycle 80/20 v/v H<sub>2</sub>/CO<sub>2</sub> through each reactor for 45 seconds and pressurize to 200 kPa.
9. Shake vigorously and place in 37°C incubator at least 5 days prior to use making sure to shake vigorously at least once each day.

#### **Preparation of General Salts solution**

Use 50 ml per 100 ml of medium (modified from Romesser et al., 1979)

<b>Composition</b>	<b>g/L</b>	<b>Medium concentration (mM)</b>
KCl	0.67	4.5
MgCl <sub>2</sub> ·6H <sub>2</sub> O	5.50	13.5
MgSO <sub>4</sub> ·7H <sub>2</sub> O	6.90	14.0
NH <sub>4</sub> Cl	1.00	9.0
CaCl <sub>2</sub> ·2H <sub>2</sub> O	0.28	0.95

### Preparation of Iron Stock solution

Use 0.5 ml per 100 ml of medium

To a small screw top bottle, add 2.0 g of  $\text{Fe}(\text{NH}_4)_2(\text{SO}_4)_2 \cdot 6\text{H}_2\text{O}$ . Then add 20 drops of concentrated HCl followed by 1000 ml of nanopure distilled water.

### Preparation of Trace minerals solution

Use 1 ml per 1 liter of medium

Composition	g/L	Medium concentration( $\mu\text{M}$ )
Nitriloacetic acid	1.5	78
$\text{MnSO}_4 \cdot 2\text{H}_2\text{O}$	0.1	5.3
$\text{Fe}(\text{NH}_4)_2(\text{SO}_4)_2 \cdot \text{H}_2\text{O}$	0.2	5.1
$\text{CoCl}_2 \cdot 6\text{H}_2\text{O}$	0.1	4.2
$\text{ZnSO}_4 \cdot 7\text{H}_2\text{O}$	0.1	3.5
$\text{CuSO}_4 \cdot 5\text{H}_2\text{O}$	0.01	0.4
$\text{NiCl}_2 \cdot 6\text{H}_2\text{O}$	0.025	1.1
$\text{Na}_2\text{SeO}_3$	0.2	11.6
$\text{Na}_2\text{MoO}_4 \cdot 2\text{H}_2\text{O}$	0.1	4.1
$\text{Na}_2\text{WO}_4 \cdot 2\text{H}_2\text{O}$	0.1	3.0

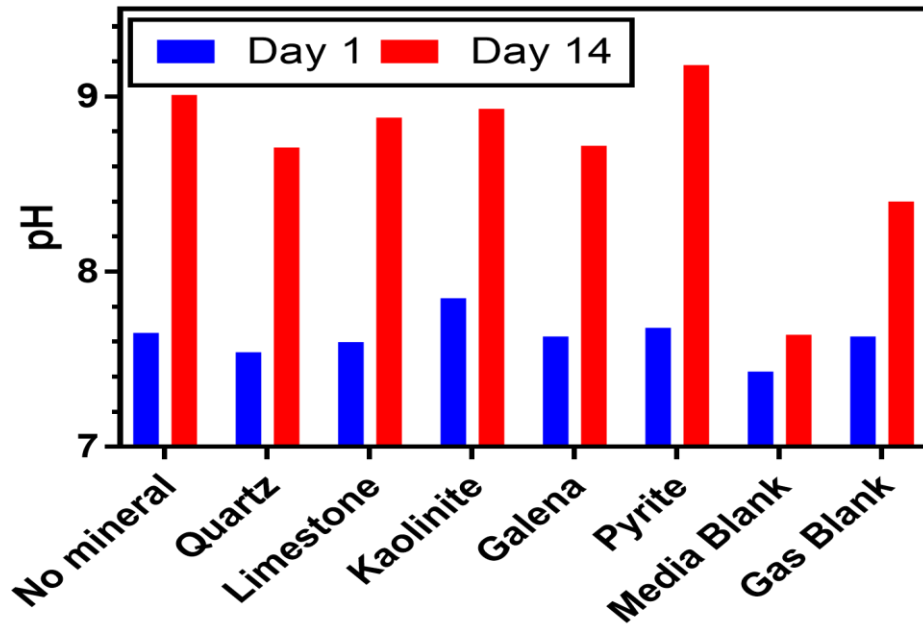
Neutralize the nitriloacetic acid to pH 6.5 with KOH, add minerals in order, allowing each one to dissolve before adding the next mineral, and adjust pH to 7.0.

### Preparation of 2.5% Sodium Sulfide solution

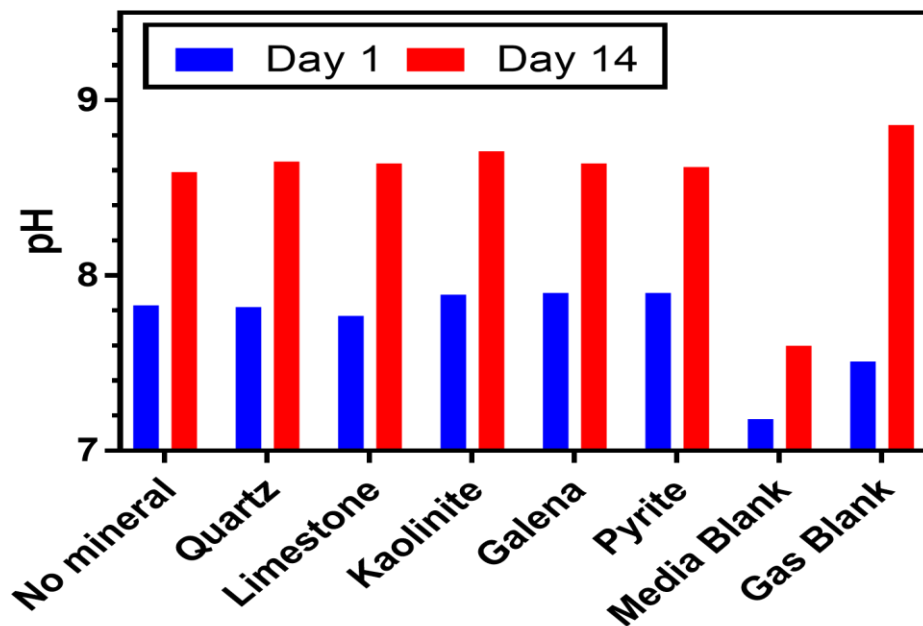
- (1) Add 100 ml nanopure H<sub>2</sub>O to flask and mark the water line. To limit the formation of volatile hydrogen sulfide from sodium sulfide, add one pellet of NaOH. Add 10 ml more nanopure H<sub>2</sub>O to flask.
- (2) Boil the 110ml nanopure H<sub>2</sub>O while flushing flask with N<sub>2</sub> until the water level reaches the marked 100 ml water line.
- (3) Let flask cool while flushing with N<sub>2</sub>, transfer the flask to the gassing station in the fume hood. Continue to flush with N<sub>2</sub>.
- (4) While flask is cooling, weigh out slightly more than 2.5 g Na<sub>2</sub>S·9H<sub>2</sub>O. Wear gloves to do the subsequent steps in the fume hood. Clean the sodium sulfide crystal by briefly rinsing the crystal with nanopure H<sub>2</sub>O followed by blotting dry with a paper towel. Re-weigh the crystal to insure the final weight is 90-110% of the desired weight.
- (5) Add the cleaned and weighted sodium sulfide to the cooled flask while flushing with N<sub>2</sub> and mix until partially dissolved.
- (6) Stopper the flask, discontinue flushing, and dispense 5ml aliquots in 28 ml Balch tubes.
- (7) Seal and crimp tubes, clear the headspace with N<sub>2</sub> gas, and pressurize to 15 psi.
- (8) Autoclave on gravity cycle for 25 minutes.
- (9) Store these sodium sulfide tubes sealed in the fume hood; Discard if precipitant forms.

Appendix B: pH values for varying mineral types in early and late stages of growth

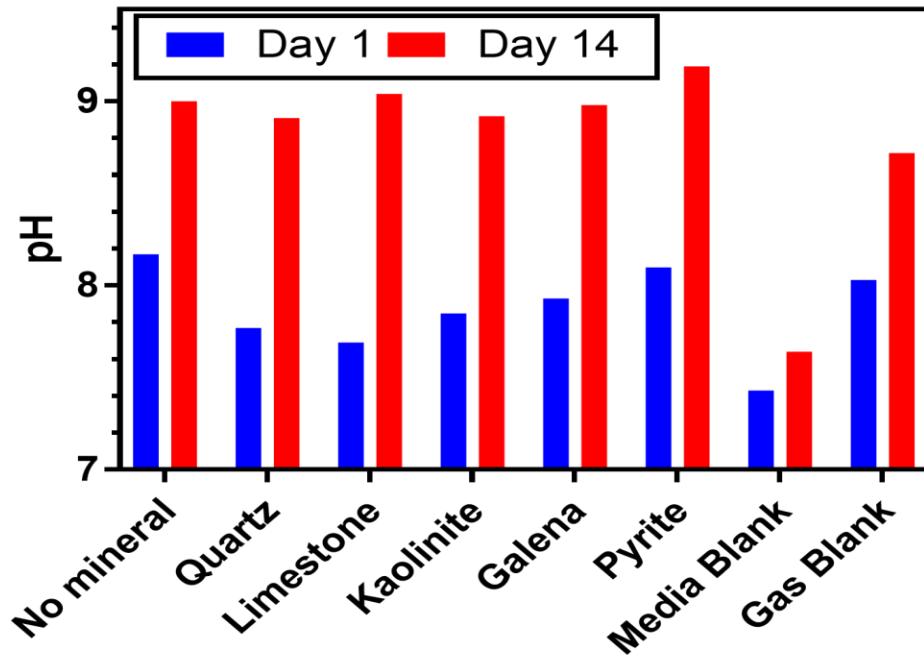
***Mm900* in H<sub>2</sub>/CO<sub>2</sub>**



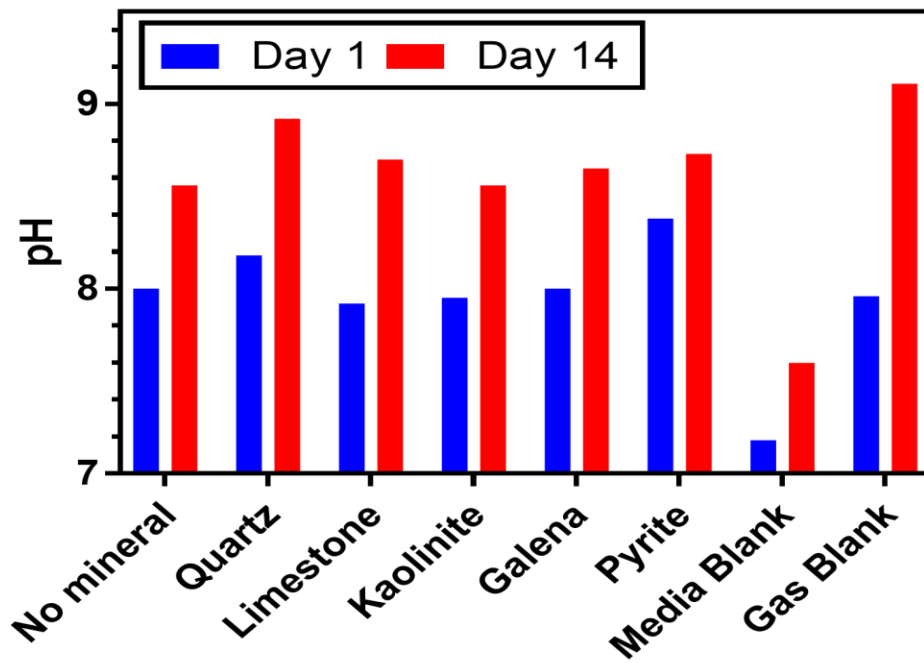
***Mm900* in N<sub>2</sub>/CO<sub>2</sub>**



### $\Delta flaB2$ in H<sub>2</sub>/CO<sub>2</sub>



### $\Delta flaB2$ in N<sub>2</sub>/CO<sub>2</sub>



### Appendix C: Overall CH<sub>4</sub> and CO<sub>2</sub> Concentrations on Day 14 (%)

---

<u>H<sub>2</sub>-rich conditions</u>	CH <sub>4</sub> (%)	CO <sub>2</sub> (%)
<u><i>Mm900</i></u>		
Galena	1.55	0.68
Pyrite	2.90	0.29
Kaolinite	6.57	0.48
Quartz	5.85	0.94
Limestone	4.01	0.47
Non-mineral	4.91	1.20
<u><i>ΔflaB2</i></u>		
Galena	2.38	0.29
Pyrite	8.81	0.18
Kaolinite	6.57	0.52
Quartz	6.47	0.49
Limestone	4.04	0.49
Non-mineral	13.2	0.27

---



---

<b><u>H<sub>2</sub>-limited conditions</u></b>	<b>CH<sub>4</sub> (%)</b>	<b>CO<sub>2</sub> (%)</b>
<b><u>Mm900</u></b>		
Galena	22.7	1.97
Pyrite	19.4	1.16
Kaolinite	18.3	1.39
Quartz	20.9	1.97
Limestone	12.9	0.96
Non-mineral	16.8	1.95
<b><u>ΔflaB2</u></b>		
Galena	14.1	0.95
Pyrite	15.3	1.04
Kaolinite	19.3	1.79
Quartz	9.23	0.12
Limestone	22.5	1.78
Non-mineral	18.9	1.65

---

## REFERENCES

- (1) Zavala, J. A.; Gog, L.; Giacometti, R., Anthropogenic increase in carbon dioxide modifies plant–insect interactions. *Annals of Applied Biology* **2017**, *170*, (1), 68-77.
- (2) Yang, G. C.; Zhou, L.; Mbadanga, S. M.; Liu, J. F.; Yang, S. Z.; Gu, J. D.; Mu, B. Z., Formate-Dependent Microbial Conversion of CO<sub>2</sub> and the Dominant Pathways of Methanogenesis in Production Water of High-temperature Oil Reservoirs Amended with Bicarbonate. *Frontiers in Microbiology* **2016**, *7*, 365.
- (3) Goldberg, D. S.; Takahashi, T.; Slagle, A. L., Carbon Dioxide Sequestration in Deep-Sea Basalt. *Proceedings of the National Academy of Sciences of the United States of America* **2008**, *105*, (29), 9920-9925.
- (4) Cuéllar-Franca, R. M.; Azapagic, A., Carbon capture, storage and utilisation technologies: A critical analysis and comparison of their life cycle environmental impacts. *Journal of CO<sub>2</sub> Utilization* **2015**, *9*, (Supplement C), 82-102.
- (5) Koornneef, J.; Ramírez, A.; Turkenburg, W.; Faaij, A., The environmental impact and risk assessment of CO<sub>2</sub> capture, transport and storage-an evaluation of the knowledge base using the DPSIR framework. *Energy Procedia* **2011**, *4*, (Supplement C), 2293-2300.
- (6) Bahrami, A.; Jamialahmadi, M.; Moghadasi, J.; Alimohammadi, N., Simulation study of CO<sub>2</sub> sequestration potential of the Mary Lee coal zone, Black Warrior basin. *Environmental Earth Sciences* **2013**, *70*, (6), 2501-2509.
- (7) Muggerridge, A.; Cockin, A.; Webb, K.; Frampton, H.; Collins, I.; Moulds, T.; Salino, P., Recovery rates, enhanced oil recovery and technological limits. *Philosophical transactions. Series A, Mathematical, physical, and engineering sciences* **2014**, 372.
- (8) Fang, Z.; Li, X.; Wang, G., A gas mixture enhanced coalbed methane recovery technology applied to underground coal mines. *Journal of Mining Science* **2013**, *49*, (1), 106-117.
- (9) Jin, C.; Liu, L.; Li, Y.; Zeng, R., Capacity assessment of CO<sub>2</sub> storage in deep saline aquifers by mineral trapping and the implications for Songliao Basin, Northeast China. *Energy Science & Engineering* **2017**.
- (10) Celia, M. A., S. Bachu, J. M. Nordbotten, and K. W. Bandilla, Status of CO<sub>2</sub> storage in deep saline aquifers with emphasis on modeling approaches and practical simulations. *Water Resour. Res* **2015**, *51*, 6846-6892.

- (11) Lau, M. C. Y.; Kieft, T. L.; Kuloyo, O.; Linage-Alvarez, B.; Van Heerden, E.; Lindsay, M. R.; Magnabosco, C.; Wang, W.; Wiggins, J. B.; Guo, L.; Perlman, D. H.; Kyin, S.; Shwe, H. H.; Harris, R. L.; Oh, Y.; Yi, M. J.; Purtschert, R.; Slater, G. F.; Ono, S.; Wei, S. W.; Li, L.; Lollar, B. S.; Onstott, T. C., An oligotrophic deep-subsurface community dependent on syntrophy is dominated by sulfur-driven autotrophic denitrifiers. *Proceedings of the National Academy of Sciences of the United States of America* **2016**, *113*, (49), E7927-E7936.
- (12) Kotelnikova, S., Microbial production and oxidation of methane in deep subsurface. *Earth Science Reviews* **2002**, *58*, (3), 367-395.
- (13) Harvey, O. R.; Qafoku, N. P.; Cantrell, K. J.; Wilkins, M. J.; Brown, C. F., Methanogenesis-induced pH-Eh shifts drives aqueous metal(loid) mobility in sulfide mineral systems under CO<sub>2</sub> enriched conditions. *Geochimica et Cosmochimica Acta* **2016**, *173*, 232-245.
- (14) Goyal, N.; Padhiary, M.; Karimi, I. A.; Zhou, Z., Flux measurements and maintenance energy for carbon dioxide utilization by *Methanococcus maripaludis*. *Microbial Cell Factories* **2015**, *14*, 146.
- (15) Capone, D. G.; Reese, D. D.; Kiene, R. P., Effects of Metals on Methanogenesis, Sulfate Reduction, Carbon Dioxide Evolution, and Microbial Biomass in Anoxic Salt Marsh Sediments. *Applied and Environmental Microbiology* **1983**, *45*, (5), 1586-1591.
- (16) Lorowitz, W. H.; Nagle, D. P.; Tanner, R. S., Anaerobic oxidation of elemental metals coupled to methanogenesis by *Methanobacterium thermoautotrophicum*. *Environmental Science and Technology* **1992**, *26*, (8), 1606-1610.
- (17) Conlette, O. C.; Emmanuel, N. E.; Chijoke, O. G., Methanogen Population of an Oil Production Skimmer Pit and the Effects of Environmental Factors and Substrate Availability on Methanogenesis and Corrosion Rates. *Microbial Ecology* **2016**, *72*, (1), 175-184.
- (18) Goyal, N.; Zhou, Z.; Karimi, I. A., Metabolic processes of *Methanococcus maripaludis* and potential applications. *Microbial Cell Factories* **2016**, *15*, (1), 107.
- (19) Jones, W. J.; Paynter, M. J. B.; Gupta, R., Characterization of *Methanococcus maripaludis* sp. nov., a new methanogen isolated from salt marsh sediment. *Archives of Microbiology* **1983**, *135*, (2), 91-97.
- (20) Jarrell, K. F.; Stark, M.; Nair, D. B.; Chong, J. P. J., Flagella and pili are both necessary for efficient attachment of *Methanococcus maripaludis* to surfaces. *FEMS Microbiology Letters* **2011**, *319*, (1), 44-50.
- (21) Lohner, S. T.; Deutzmann, J. S.; Logan, B. E.; Leigh, J.; Spormann, A. M., Hydrogenase-independent uptake and metabolism of electrons by the archaeon *Methanococcus maripaludis*. *ISME Journal* **2014**, *8*, (8), 1673-1681.

- (22) Sydow, A.; Krieg, T.; Mayer, F.; Schrader, J.; Holtmann, D., Electroactive bacteria—molecular mechanisms and genetic tools. *Applied Microbiology and Biotechnology* **2014**, *98*, (20), 8481-8495.
- (23) Bandara, W.; Kindaichi, T.; Satoh, H.; Sasakawa, M.; Nakahara, Y.; Takahashi, M.; Okabe, S., Anaerobic treatment of municipal wastewater at ambient temperature: Analysis of archaeal community structure and recovery of dissolved methane. *Water Research* **2012**, *46*, (17), 5756-5764.
- (24) Feng, Y. H.; Zhang, Y. B.; Quan, X.; Chen, S., Enhanced anaerobic digestion of waste activated sludge digestion by the addition of zero valent iron. *Water Research* **2014**, *52*, 242-250.
- (25) Takeshita, T., A cost-optimal scenario of CO<sub>2</sub> sequestration in a carbon-constrained world through to 2050. *Natural Science* **2013**, *5*, (2), 313-319.
- (26) Kato, S.; Hashimoto, K.; Watanabe, K., Methanogenesis facilitated by electric syntrophy via (semi)conductive iron-oxide minerals: Methanogenesis via (semi)conductive minerals. *Environmental Microbiology* **2012**, *14*, (7), 1646-1654.
- (27) Zhou, S.; Xu, J.; Yang, G.; Zhuang, L., Methanogenesis affected by the co-occurrence of iron(III) oxides and humic substances. *FEMS Microbiology Ecology* **2014**, *88*, (1), 107-120.
- (28) Jiang, S. H.; Park, S.; Yoon, Y.; Lee, J. H.; Wu, W. M.; Dan, N. P.; Sadowsky, M. J.; Hur, H. G., Methanogenesis Facilitated by Geobiochemical Iron Cycle in a Novel Syntrophic Methanogenic Microbial Community. *Environmental Science and Technology* **2013**, *47*, (17), 10078-10084.
- (29) Malvankar, N. S.; King, G. M.; Lovley, D. R., Centimeter-long electron transport in marine sediments via conductive minerals. *ISME Journal* **2015**, *9*, (2), 527-531.
- (30) Qiao, S.; Tian, T.; Qi, B.; Zhou, J., Methanogenesis from wastewater stimulated by addition of elemental manganese. *Scientific Reports* **2015**, *5*, 12732.
- (31) Palacky, G. J., Resistivity Characteristics of Geologic Targets. *Electromagnetic Methods in Applied Geophysics* **1983**, 52-129.
- (32) Pridmore, D. F. a. S. R. T., The electrical resistivity of galena, pyrite, and chalcopyrite. *American Mineralogist* **1976**, *61*, 248-259.
- (33) Belay, N.; Daniels, L., Elemental metals as electron sources for biological methane formation from CO<sub>2</sub>. *Antonie van Leeuwenhoek International Journal of General and Molecular Microbiology*. **1990**, *57*, (1), 1-7.

## VITA

### Personal Background

Patrick Bond Lazzarino  
Hattiesburg, Mississippi  
Son of John and Tammy Lazzarino  
Not married

### Education

Bachelor of Science, Business Administration,  
University of Southern Mississippi, 2010  
Bachelor of Science, Geology, University of Southern  
Mississippi, 2015  
Master of Science, Environmental Science, Texas  
Christian University, 2017

### Experience

Operations Manager, Maaco Collision and Auto Repair,  
2008-2015, Hattiesburg  
Teaching Assistant, Texas Christian University,  
2016-2017

## ABSTRACT

### CO<sub>2</sub> TO NATURAL GAS (CH<sub>4</sub>) CONVERSION IN METHANOGEN-MINERAL SYSTEMS: THE ROLE OF MINERAL TYPE

by Patrick Bond Lazzarino, M.S., 2017  
Department of Environmental Science  
Texas Christian University

#### Thesis Advisors:

Omar R. Harvey, Assistant Professor of Environmental Science

William B. Whitman, Professor of Microbiology, University of Georgia

Kayla N. Green, Associate Professor of Chemistry

Although the mechanisms are not completely understood, the need for both archaella and pili for attachment of *Methanococcus maripaludis* to mineral surfaces has been well established. In addition, the uses for these pili and/or archaella are still not completely understood, but it has been proposed that they could function to preferentially attach to conductive surfaces allowing for electron shuttling. In reactors containing minerals of varying mineral electrical conductivity -pyrite >galena >kaolinite >quartz>limestone-wildtype *M. maripaludis* (*Mm900*) and non-archaellated mutant ( $\Delta$ *flaB2*) were examined in H<sub>2</sub>-rich and H<sub>2</sub>-limited environments to determine trends in early-stage methanogenesis. Building on these trends, a kinetic model of these early-stage trend was created based on the fitted parameters (*c*, *k*, and *t*<sub>1/2</sub>).